Nanoscale

REVIEW

View Article Online
View Journal | View Issue

Cite this: *Nanoscale*, 2024, **16**, 22077

Single atoms meeting 2D materials: an excellent configuration for photocatalysis

Yameng He,[a] Yi Zhang,*[b] Gazi Hao,*[a] Wei Jiang[a] and Jun Di*[a]

Received 15th September 2024,
Accepted 24th October 2024

DOI: 10.1039/d4nr03787a

rsc.li/nanoscale

Photocatalysis has problems such as low light absorption efficiency and rapid recombination of photogenerated electron–hole pairs. Many studies have been conducted to improve these issues. This review encapsulates the progress and applications of two pioneering research fields in catalysis: single-atom and two-dimensional (2D) material catalysts. The advent of this new type of catalysts, which integrates single atoms onto 2D materials, has seen remarkable growth in recent years, offering distinctive advantages. The article delves into the array of synthesis methods employed for loading single atoms onto 2D materials, including the wet chemical approach, atomic layer deposition technique, and thermal decomposition method. A highlight of the review is the superior attributes of single-atom catalysts supported on 2D materials (SACs-2D) in photocatalysis, such as extending the light absorption wavelength range, enhancing the efficiency of photogenerated electron–hole pair separation, and accelerating redox kinetics. The review meticulously examines the diverse applications of SACs-2D photocatalysis, which encompass water splitting for hydrogen generation, carbon dioxide reduction, degradation of organic pollutants, nitrogen fixation and hydrogen peroxide synthesis. These applications demonstrate the potential of SACs-2D materials in addressing pressing environmental and energy challenges. Finally, this article evaluates the current state of this burgeoning field, discussing the opportunities and challenges ahead.

[a]*School of Chemistry and Chemical Engineering, National Special Superfine Powder Engineering Research Center, Nanjing University of Science and Technology, Nanjing, 210094, China. E-mail: hgznjust1989@163.com, dijun@njust.edu.cn*
[b]*Department of Applied Physics, The Hong Kong Polytechnic University, Hung Hom, Hong Kong, P. R. China. E-mail: yes.zhang@polyu.edu.hk*

Jun Di

Jun Di received his BS degree (2012) and PhD degree (2018) from Jiangsu University. He then carried out postdoctoral research (2018–2022) at Nanyang Technological University with Professor Zheng Liu. He is currently a professor at Nanjing University of Science and Technology and selected as a national overseas high-level young talent. He is the first or corresponding author of more than 80 peer-reviewed scientific papers published in Nat. Commun., Coord. Chem. Rev., Adv. Mater., Angew. Chem. Int. Ed., Mater. Today, etc., *with over 15 000 citations and H-index 66. His research interests focus on the design of 2D materials for photocatalytic energy conversion.*

1. Introduction

Currently, the majority of the global energy demand is satisfied by fossil fuels, accounting for 85% of the world's total energy consumption.[1] However, the finite reserves of these fuels and the escalating environmental concerns caused by excessive greenhouse gas emissions underscore their long-term unsustainability. Solar energy, celebrated for its abundant resources, cleanliness, and perpetual sustainability, has emerged as an appealing alternative.[2] Photocatalysis is a process that harnesses light energy to facilitate the conversion of substances, involving a chemical reaction that is both light- and catalyst-dependent. Specifically, in photocatalysis, semiconductor catalysts are activated by solar energy, generating photogenerated electron–hole pairs.[3] These pairs then migrate to the surface of the catalyst, triggering reduction and oxidation reactions. The photocatalytic process comprises three crucial stages: light absorption, separation of photogenerated carriers, and interfacial catalytic reactions.[4] The utilization of solar energy for photocatalysis holds great promise in addressing current energy requirements while mitigating environmental issues associated with conventional fuel sources. This technology offers a viable path towards a sustainable and eco-friendly future.

In the quest to harness photocatalysis for energy conversion and environmental remediation, there has been an unwavering

pursuit of photocatalysts that possess not only robust active sites but also superior light-harvesting efficiency, reduced electron–hole recombination rates, and heightened catalytic efficacy. Despite these aspirations, traditional photocatalytic systems have faced obstacles, including a rapid carrier recombination rate and limited active sites.[5,6] These limitations result in low light energy conversion efficiency and an insufficient selectivity for target products. In recent years, various research teams have endeavored to surmount these challenges through innovative approaches. Within the realm of nanomaterials, two-dimensional (2D) materials have emerged as a promising class of substances, characterized by their sheet-like structures consisting of thick layers of single or several atoms. They are a wide range of materials applied in multiple domains, such as energy conversion and storage,[7–9] optoelectronics,[10–12] and catalysis.[13–19] The inherent advantages of 2D materials include: (1) a pronounced surface area that provides an abundance of surface-active sites for catalytic processes; (2) lower atomic escape energy on the surface of the material, which facilitates the formation of defect sites. The existence of surface defects is conducive to the adsorption of molecules or atoms, thereby enhancing the redox process; (3) preponderance of surface low-coordination atoms, which elevates the likelihood of active sites engaging in reactive processes; (4) the ultrathin 2D structure that exhibits superior UV-visible light absorption capabilities, obviating the constraints imposed by the transmittance and reflection characteristics of bulk materials; and (5) the ultrathin thickness greatly shortens the diffusion distance of carriers, greatly reducing the possibility of recombination of photogenerated carriers and then facilitating the photocatalytic process. Currently, 2D materials such as graphitic carbon nitride (g-C_3N_4),[20–30] graphene,[31] TiO_2 nanosheets,[32–35] iron oxide nanosheets,[36] $Bi_{24}O_{31}Br_{10}$,[37] $ReSe_2$ [38] and $Znln_2S_4$ [39] exhibit good performance in photocatalysis. Nevertheless, the performance of 2D materials is still far from the requirements of industrial applications. For example, while some 2D materials may have many surface sites, their activity is suboptimal, thus compromising the efficiency of photocatalytic reactions. Besides, the light absorption range of some 2D materials may be limited to a narrow range of wavelengths, resulting in lower efficiency when absorbing other wavelengths of light. To address these issues, various surface and interface engineering strategies have been employed to further enhance their photocatalytic performance.

In the field of contemporary catalysis research, single-atom catalysts (SACs) have garnered considerable prominence due to their exceptional catalytic efficacy.[3] SACs shrink metal nanoparticles to the point where a single atom can fully expose the phase interface, giving them some compelling advantages: (1) they have a potential ultrahigh atom utilization efficiency of up to 100%, which can significantly enhance photocatalytic activity; (2) the single atoms can act as active sites, providing additional reactive sites and thus enhancing the photocatalytic performance[40] and (3) they are highly tunable, with a wide variety of single atoms, which can provide sufficient light-trapping ability and precise surface modification for adsorption and activation of molecules. For example, Zhang *et al.* found that[41] the active site of Zn can effectively activate nitrogen-containing molecules and promote C–N coupling, and in particular, after the introduction of Zn monoatoms, the catalytic activity of single atom catalysts (SACs) can be maximized due to their high atom utilization and unique electron/coordination configurations. The Zhang team[42] designed single atom Ce sites loaded on nitrogen doped hollow carbon spheres, achieving high-performance conversion of NO to NH_3. Since both 2D materials and single atoms have irreplaceable advantages and complementary strengths in photocatalysis, many teams have explored their integration to improve photocatalytic performance. This amalgamation has led to significant breakthroughs in the field, as the incorporation of single atoms onto 2D materials can effectively mitigate certain limitations inherent to the 2D materials themselves, thereby enhancing photocatalytic performance and facilitating the photocatalytic reaction process. For instance, the integration of single atoms can regulate the optical properties of 2D materials, expand the light absorption spectrum, and ultimately enhance photocatalytic efficiency. Moreover, 2D materials can enhance the stability of single-atom loads, reduce the deactivation phenomenon in the photocatalytic process, and prolong the service life of the materials.

Multiple endeavors have been made to accelerate the progression of single atom catalysts supported on two-dimensional (SACs-2D) material technology. Previous research or perspectives on SACs-2D materials primarily concentrated on specific materials or restricted applications. For instance, in 2020, Jiao's team summarized the underlying principles and obstacles encountered in the utilization of ultrathin 2D photocatalysts for CO_2 photoreduction, with an introduction to enhance the kinetics of redox reactions induced by the combination of isolated single atoms with ultrathin 2D semiconductors.[43] A schematic diagram of three forms of single atom loaded two-dimensional materials is given (Scheme 1): lattice doping; surface connection; connected through ligands. Despite the significant progress made in SACs-2D materials technology, there are still some issues that need to be taken care of for further investigation and resolution to fully exploit the potential of these materials.

This review introduces the latest progress in various photocatalytic applications of single atom supported 2D material catalysts. It systematically appraises the methodologies employed for the integration of single atoms onto 2D materials, including wet chemistry methods, atomic layer deposition techniques, and thermal decomposition methods. The review highlights the pivotal role of SACs-2D materials in the photocatalytic process. Furthermore, various applications of SACs-2D materials in photocatalysis have also been introduced, including water splitting for hydrogen generation, carbon dioxide reduction, decomposition of organic contaminants, hydrogen peroxide synthesis, and nitrogen fixation. Finally, we provide an outlook on the ongoing challenges and future outlook of SACs-2D materials in photocatalysis. At present, most of the existing reviews discuss single atom cata-

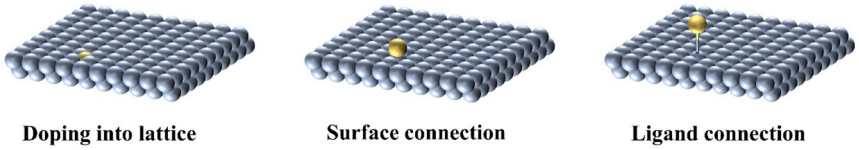

Scheme 1 Schematic diagram of three forms of SACs-2D materials.

lysts or 2D materials separately, and there are no reviews that focus on the development of the combination of single atoms and 2D materials in the field of photocatalysis. This review aims to demonstrate the development of the combination of two materials (single atoms and 2D) with excellent photocatalytic performance and provide ideas for the future development of such materials.

2. Synthesis of SACs-2D materials

For the synthesis of SACs-2D materials, various methodologies lead to diverse microstructures and active sites, thereby exerting a crucial influence on their photocatalytic capabilities. The essence of SACs-2D materials synthesis lies in the precise anchoring of isolated atoms onto the surface of the two-dimensional support material.[44] Currently, the predominant methods available for the synthesis pathway are wet chemistry, atomic layer deposition and thermal copolymerization. Wet chemistry and thermal copolymerization belong to bottom-up methods, which construct material structures by gradually assembling atoms or molecules together; Atomic layer deposition belongs to the top-down method, which involves depositing atomic layers onto the substrate surface to control the thin film growth and structural formation of the material. Each of these methods has its unique advantages, which are discussed comprehensively in the following sections.

2.1 Wet chemical routes

The wet chemical route stands out as a frequently adopted method for depositing single atoms on the carrier surface of 2D materials, which generally consists of two pivotal steps: initially, a suitable quantity of metal precursor is anchored onto the carrier surface by impregnation, adsorption, ligand-bonding or deposition; subsequently, to facilitate the transition of the surface-bound precursor into firmly anchored single atoms on the carrier surface, appropriately designed reduction and activation procedures are implemented. Wet chemical methods involve the synthesis of materials by chemical reactions at lower temperatures using liquid phase media such as water or organic solvents. These methods include chemical reduction deposition, sol–gel synthesis, hydrothermal crystallization, precipitation synthesis, *etc*. They are noted for their simplicity, low cost, and easy control of reaction conditions, and can be used to prepare a diverse array of functional materials.

For the synthesis of Mo-PCN, a wet chemical method[22] involves dissolving urea in double distilled water, followed by the addition of $Na_2MoO_4{\cdot}H_2O$, then stirring, dehydration using a rotary evaporator, calcination, washing, and drying to yield the Mo-PCN catalyst (Fig. 1a). In the research of monatomic Ru modified TiO_2 nanosheets,[32] Liu *et al.* used the gel–sol method to prepare Ru-TiO_2 nanosheets. This process began with dispersing the acquired TiO_2 nanosheets in ethanol, followed by the gradual addition of a rhodium chloride hydrate ethanol solution, with continuous stirring for 6 hours. The resultant precipitate was filtered, washed extensively with distilled water, and dried under vacuum at 60 °C to produce high-purity Ru-TiO_2 nanosheets. These nanosheets were then heat-treated in a tube furnace at 250 °C for 2 hours. Su *et al.* synthesized a single-atom Pt^{II}-C_3N_4 catalyst by the chemical reduction deposition method using $H_2PtCl_6{\cdot}4H_2O$ and g-C_3N_4 suspension.[23] Huang[45] mixed $CoCl_2$ and C_3N_4 in acetonitrile, then heated the mixture with triethylamine (TEA) to deposit Co^{2+} sites on C_3N_4. Immersion is a straightforward technique for synthesizing single-atom catalysts on 2D materials (SACs-2D), where a solution containing active metal precursors is mixed with a catalyst carrier to affix the precursors *via* ion exchange or adsorption. For example, Chen *et al.*[3] successfully loaded single atom Pt onto defective TiO_2 through impregnation, with a loading content of 0.02 wt%. The co-precipitation method, another wet chemical technique, is used to prepare mixed metal oxides or other complexes by precipitating two or more different metal ions simultaneously in solution. This method is frequently employed in the synthesis of multi-component photocatalysts. M-TiO_2 (M = Pt, Pd, Rh) were synthesized by the co-precipitation method.[46] Through the precise regulation of H_2PtCl_6 in the aqueous dispersion of g-C_3N_4 nanosheets, the $PtCl_6^{2-}$ ions were effectively transformed into individual Pt atoms and then fixed onto the carriers, and single-atom Pt was successfully loaded onto g-C_3N_4 nanosheets by a simple green process of *in situ* photodeposition. In the study of modulating the specific coordination environment of Pt single atoms,[27] this wet chemistry method is also applied by Zhai and colleagues to load single-atom Pt onto N-vacancy-rich g-C_3N_4 carriers.

2.2 Atomic layer deposition

Atomic layer deposition (ALD) is an advanced technique used to deposit thin films through a controlled layer-by-layer material accretion process. In ALD, two gas-phase precursors are alternately injected into a reaction chamber to interact with the substrate surface and deposit a thin film. Then the unreacted gas-phase precursor is discharged from the chamber and another

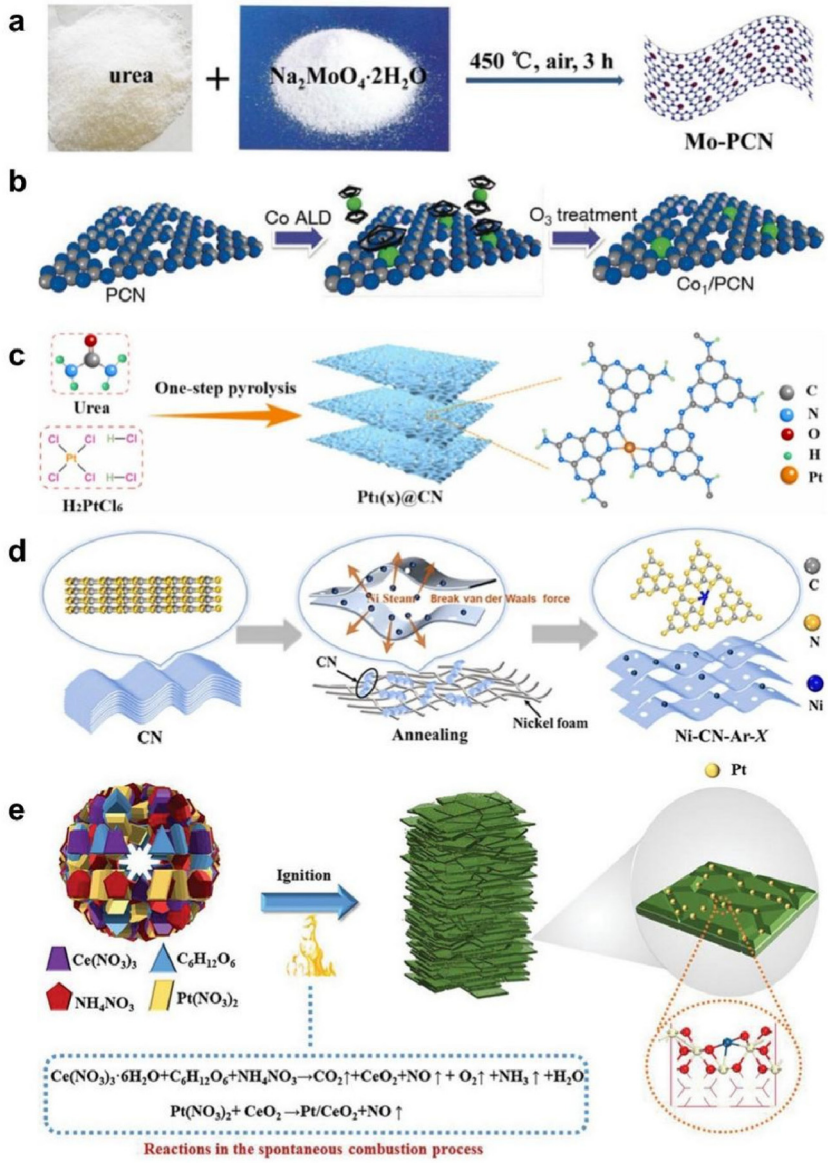

Fig. 1 (a) Wet chemical synthesis of Mo-PCN-SACs. Reproduced with permission.[22] Copyright 2019, Royal Society of Chemistry. (b) ALD method for synthesizing unit point Co_1/PCN catalysts. Reproduced with permission.[48] Copyright 2017, Wiley-VCH. (c) Pyrolysis synthesis of Pt1(*x*)@CN. Reproduced with permission.[50] Copyright 2024, Elsevier. (d) Metal vapor exfoliation synthesis of Ni-C_3N_4. Reproduced with permission.[52] Copyright 2024, Elsevier. (e) Schematic diagram of 2D CeO_2 supported atomic Pt catalysts prepared using the precursor combustion strategy. Reproduced with permission.[53] Copyright 2024, Wiley-VCH.

gas-phase precursor is introduced, and so on until the desired film thickness is achieved. Characterized by its repetitive nature, ALD fundamentally hinges on a sequential electrochemical approach, which involves the orchestrated interaction of gaseous components with a surface. This technique parallels the principles of chemical vapor deposition, in that the film's thickness can be precisely regulated by manipulating the quantity, sequence, and diversity of atomic layer deposition cycles. Hence, ALD offers a high degree of control over film thickness and composition.[47]

Cao *et al.*[48] prepared single atom Co composite materials using ALD technology (Fig. 1b). Firstly, g-C_3N_4 was synthesized using urea as a precursor using a typical thermal shrinkage method. Before depositing Co, phosphating treatment was performed on g-C_3N_4 to enhance carrier separation and transfer in its photocatalytic reaction. Bis(cyclopentadienyl)cobalt, Co $(Cp)_2$ was used for Co ALD, subsequently the material underwent an O_3 treatment for a brief duration of 150 seconds and comparatively low temperature to eliminate the ligand Cp, ultimately synthesizing Co-C_3N_4.

2.3 Pyrolysis method

Pyrolysis stands as a prevalent technique among the methods for synthesizing SACs-2D materials. The pyrolysis method

refers to dispersing metal precursors through spatial constraints, and then reducing the initial reactive component through elevated temperature processing for producing single atom catalysts *in situ*. The main steps of the pyrolysis method include the following aspects: first, selecting suitable precursors, then pyrolysis treatment, and finally loading them on a stable 2D material carrier. In general, the synthesis of SACs by the pyrolysis method has the advantages of simplicity and efficiency. It can prepare SACs-2D materials with high specific surface area and good catalytic performance, which is of great significance for promoting the development of the catalyst field.

In the study of single atom Co loaded g-C_3N_4 for water splitting hydrogen production, Shi *et al.*[49] employed a new *in situ* synthesis method to prepare high metal loaded single cobalt atom catalysts, as traditional synthesis methods typically provide extremely low metal loads. This novel approach involved the utilization of nitrogen-rich molecular carbon precursors (1,4,5,8,9,12-hexaazaphenylhexacarbonitrile) and $CoCl_2$, synthesized through a one-step pyrolysis method, resulting in the fixation of a single cobalt atom catalyst onto a porous nitrogen-doped carbon carrier. Based on the successful electron migration from g-C_3N_4 to Co SA, high-performance photocatalytic hydrogen production has been achieved. Additionally, Pt single atom anchored porous C_3N_4 nanosheet photocatalysts (Pt1(x)@CN, where x represents the weight percentage of Pt content) were fabricated using a straightforward single-step pyrolysis technique[50] (Fig. 1c). Ce-SA-C_3N_4 was prepared by high-temperature decomposition of Ce doped lamellar supramolecular precursors to prepare Ce single atom incorporated C_3N_4 nanosheets.[26] Subsequently, ultrasound treatment was performed to obtain ultra-thin C_3N_4 nanosheets loaded with single atom Ce (Ce-SA-C_3N_4). Zhao *et al.* used[51] MOFs to achieve atomic separation and immobilized metal single atoms through the abundant coordination sites generated by MOFs after pyrolysis.

2.4 Other methods

There are many other methods to synthesize SACs-2D materials, such as metal vapor exfoliation, photodeposition and precursor combustion. Metal vapor exfoliation is a technique used to produce thin layers of metal films or nanoparticles. In the metal vapor exfoliation method, a metal source is evaporated by heating to become a metal vapor, and then the metal vapor is transported to a substrate, where it is layered on the surface of the base material to form a metal film or nanoparticles. Typically, the metal source is heated to a high temperature to evaporate and form a metal gas, and then the metal gas is transported to the surface of the substrate to deposit a metal film on the substrate. Ma *et al.*[52] loaded monoatomic Ni onto ultrathin C_3N_4 nanosheets by metal vapor exfoliation (Fig. 1d). Photodeposition is a method of depositing thin films or particles on the surface of a material using photocatalysis. Wu's team used photodeposition to decorate Pt single atoms on TiO_2 nanosheets.[33] Precursor combustion is a chemical reaction in which a compound decomposes under conditions of being heated to produce gases and solid products. The precursor combustion strategy is a simple one-step synthesis compared to conventional synthesis strategies that require complex steps and longer time to synthesize the catalysts. Dong *et al.*[53] synthesized 2D CeO_2 loaded atomic Pt catalysts by a one-step precursor combustion method (Fig. 1e).

3. Role of SACs-2D structure in photocatalysis

SACs-2D materials exhibit significant advantages in the field of photocatalysis. The distinct planar architecture of 2D nanosheets affords an optimal substrate for the anchoring of single atoms, with their surfaces providing an ideal platform for maximizing reactant exposure. Theoretically, this configuration ensures that the single atoms are optimally accessible to reactants. Upon anchoring single atoms onto 2D materials, the emergence of novel electronic states enhances its functional attributes, including the light absorption spectrum, carrier separation efficiency and redox kinetics, thus facilitating the photocatalytic process.

3.1 Expanding the wavelength range of light absorption

Light absorption is the initial and pivotal step of photocatalysis, which determines the ability of the photocatalytic system to capture incoming photons to spawn enough electron–hole pairs for the following catalytic transformations. The spectral composition of the natural sunlight spectrum encompasses approximately 5% ultraviolet light ranging from 300 to 400 nm, 43% visible light spanning 400 to 700 nm, and 52% infrared light extending from 700 to 2500 nm. Consequently, realizing the capture of visible or infrared light is crucial for maximizing the utilization of solar energy.[54] One effective approach to improve photocatalytic efficiency is to expand the wavelength range of light absorption, thus facilitating the absorption of a greater number of photons. When single atoms are integrated in 2D materials, the electronic and energy band structures of the SACs-2D materials can be tailored to absorb incoming light within designated spectral ranges, especially in the visible/infrared region, thus improving the photocatalytic capability. For this reason, researchers have paid considerable attention to the advancement of single-atom photocatalysts.

The light absorption capacity is mainly influenced by the band structure. The electronic band structure of two-dimensional materials determines their ability to absorb light of different wavelengths. If the band structure of a material matches the energy of light, light absorption will occur. The incorporation of single atoms has the potential to adjust the band structure, thereby affecting catalytic performance. The ability of single-atom-loaded 2D materials to broaden light absorption is mainly due to the interaction between SACs and 2D materials and the resulting changes in charge-carrier dynamics, energy-band structure, and interfacial states. Together, these effects improve the response and utilisation

efficiency of the materials to light. For example, during the investigation of single atom Ag modified g-C_3N_4 in the presence of peroxymonosulfate, it was found that the band gap energies of 1%, 2%, 3.5%, 5%, and 10% Ag/mpg-C_3N_4 were 2.50, 2.42, 2.39, 2.33, and 2.09 eV, respectively, which were lower than the band gap energy of g-C_3N_4, which was 2.65 eV (Fig. 2a and b). The research demonstrates that the incorporation of single atom Ag narrows the Ag/mpg-C_3N_4 band gap. Thus, it is able to absorb other photons with lower energies, which is manifested in the enhancement of visible light absorption capacity.[25] Similarly, in first-principles analysis of charge carrier dynamics in transition-metal single atoms doped g-C_3N_4, the bandgap values of Fe/g-C_3N_4 and Co/g-C_3N_4 were reduced to 1.01 and 0.72 eV, respectively (Fig. 2c–e). This means that the energy gap between the conduction band and valence band has diminished, simplifying the process for carriers to move from the valence band to the conduction band and move further in the conduction band, thereby extending their migration distance. The presence of transition metals Fe and Cu enhances the light absorption capacity of g-C_3N_4, thereby boosting its photocatalytic capabilities.[55] Single atom Co is loaded on the Bi_3O_4Br atomic layer for CO_2 photoreduction.[56] After single atom Co doping, a Co doping level is formed in the bandgap of Bi_3O_4Br, which can improve the absorption capability during the frequency range of visible light. Ma *et al.*[52] used UV-vis absorption spectral analysis to analyze the optical properties of the samples and found that the light absorption of Ni-C_3N_4 increased at 350–380 nm. This enhancement is typically ascribed to the π–π* electronic transition, indicating a more effective utilization of light energy within this specific wavelength range. In addition, upon the integration of single-atom Ni, the light absorption range of Ni-C_3N_4 significantly expanded, spanning from 464.3 nm to 556.8 nm. Compared to pure CN, the light absorption range is increased, so the introduction of single atom Ni greatly improves the absorption and utilization of visible light, thereby enhancing the overall photocatalytic performance. During the research of nitrogen fixation using single atom B-modified g-C_3N_4,[21] the band gap of pure g-C_3N_4 is 2.98 eV, and light adsorption is restricted to shorter wavelengths. With the modification of B atoms, the band gap energy has diminished to 1.12 eV, which enables B/g-C_3N_4 to capture longer wavelengths of light. Therefore, B/g-C_3N_4 has a superior light conversion efficiency than pure g-C_3N_4, ensuring a more effective yield of photoexcited electrons and an improved photocatalytic capability. Luo *et al.*[57] prepared photocatalysts by thermal polymerization and evaluated the band gap of Nb-C_3N_4 by UV-vis diffuse reflectance spectroscopy, which shifted the UV-vis absorption spectra of Nb-C_3N_4 compared to g-C_3N_4, suggesting that the incorporation of Nb into g-C_3N_4 appears to have broadened the range of wavelengths absorbed. Si *et al.* introduced[58] single atom Au into ultra-thin $ZnIn_2S_4$ for photocatalytic reduction of CO_2. The study found that the introduction of single atom Au expanded the wavelength range of light absorption, exhibited rapid carrier transfer, and thus improved the reaction performance. The Chen team[59] anchored Au single atoms in unsaturated Mo atoms of MoS_2 using salt templates and photodeposition methods, and found that light absorption was significantly enhanced, thereby promoting CO_2 reduction. Until today, the specific working mechanism of how single atoms change the light absorption ability of materials is still under study, therefore, further research on the role of SACs-2D structure in photocatalysis is necessary. Single atom loading on 2D materials enhances light absorption efficiency and promotes photocatalytic applications by improving light absorption capacity, broadening absorption

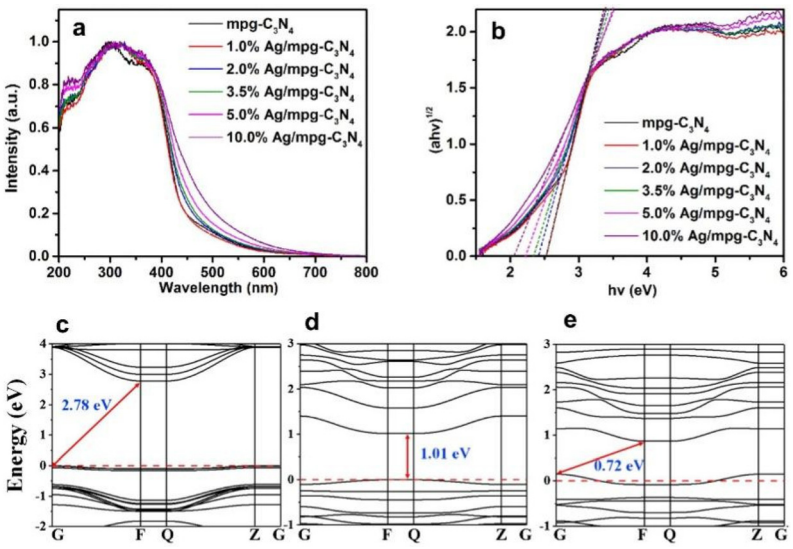

Fig. 2 The UV-vis diffuse reflectance spectra (a) Tauc plots (b) of Ag/mpg-C_3N_4 with varying Ag loading amounts. Reproduced with permission.[25] Copyright 2017, Elsevier. The energy band structures of (c) pristine g-C_3N_4, (d) Fe/g-C_3N_4, and (e) Co/g-C_3N_4. Reproduced with permission.[55] Copyright 2018, Elsevier.

range, and structural influence. Integrating a single atom into a 2D material can not only significantly improve light absorption efficiency, but also expand the spectral range of light absorption, which is of great significance for improving photocatalytic performance. By precisely regulating the electronic and band structure of SACs-2D materials, it is possible to optimize the absorption of specific wavelengths of light, thereby enhancing the material's utilization efficiency of light energy.

3.2 Improve carrier separation efficiency

In the realm of photocatalytic reactions, the effective separation of electron–hole pairs on photocatalysts plays a vital role in determining their overall photocatalytic efficiency. Within semiconductors, the migration pattern of charge carriers is generally stochastic in nature, which can result in a greater chance of carrier recombination.[43] The lifetime of carrier recombination typically falls within the range of picoseconds to nanoseconds.[60] Therefore, the lack of a driving force results only in a minimal number of electrons and holes being separated efficiently, thereby impeding the transfer of charges to the semiconductor surface and subsequently constraining the ensuing surface redox reactions. Many studies have been undertaken to reduce the recombination rate of electron–hole pairs, and it has been found that combining single atoms with 2D materials is capable of enhancing the effectiveness of carrier separation. The SACs-2D materials photocatalytic system can promote effective separation of photogenerated electrons and holes through various mechanisms such as local charge enrichment, charge transfer channels, and reactive metal–support interactions (RMSI) effect, thereby improving the efficiency and selectivity of photocatalytic reactions. The first mechanism is local charge enrichment, which refers to the formation of a local negative charge region in certain specific areas of the catalyst due to the excitation of electrons after light absorption, resulting in an increase in electron density. The presence of local charges generates an electric field, which drives the migration of charges and improves the separation efficiency of electrons and holes. The second mechanism: charge transfer channel refers to the pathways and processes involved in the effective separation and transport of photogenerated electrons and holes in photocatalytic reactions. By designing charge transfer channels reasonably, including using heterostructures, optimizing band matching, constructing conductive networks, and utilizing internal and external electric fields, the separation efficiency of photogenerated electrons and holes can be effectively improved. The third mechanism, reactive metal–support interactions (RMSI), refers to the chemical interactions that occur between metal particles and carriers. The interaction between the metal and the carrier can affect the coordination environment of metal atoms, and charge transfer may also occur between the metal and the carrier, causing changes in the oxidation state of the metal and promoting charge separation. Through the above mechanism, SACs-2D materials can achieve efficient photocatalytic reactions, improving the efficiency and selectivity of photocatalysis.

In the study of single-atom Mo loaded on polymeric carbon nitride (PCN) for photocatalytic nitrogen fixation,[22] the average radiative lifetime of Mo-PCN was significantly smaller than that of PCN based on time-resolved fluorescence kinetic measurements, indicating a decrease in the excited state residence time, suggesting that photoexcited state electrons were efficiently transferred from the PCN to the Mo centers, thereby improving the efficiency of separating photoinduced electron–hole pairs. Su and colleagues[23] studied the photocatalytic water splitting reaction of Pt^{II}-C_3N_4 and found that the PL signal of Pt^{II}-C_3N_4 was significantly lower. This indicates that the collection of photocarriers in Pt^{II}-C_3N_4 is more effective, the Pt^{II}-C_3N_4 integrated structure significantly reduces the transfer barrier of photogenerated carriers and accelerates the transfer of carriers relative to g-C_3N_4, which can effectively inhibit electron–hole recombination, and promote the division and relocation of photocarriers. In the study of using ionic liquids and Co single atoms to improve CO_2 reduction,[61] the optimized photocatalyst has a CO_2 conversion rate of 42 times that of g-C_3N_4, and its selectivity for CO_2 reduction is close to 100%. Both experimental results and theoretical simulations confirm that single atom Co has the ability to extract holes to promote charge separation and catalyze water oxidation. Adopting *in situ* μs-TAS it was determined that the electron–hole pair separation efficiency in the photocatalytic reduction of CO_2 of IL-Co/g-C_3N_4 was 35.3%, which is 93 times greater than g-C_3N_4. In the Ce-SA-C_3N_4 photocatalytic reaction process,[26] single atom Ce-N_4/O_6 sites can function as extra trap states to capture photogenerated electrons, enhance electron–hole separation, and consequently boost the photocatalytic performance. The novel 2D material SiP[62] is used for photocatalytic hydrogen production, the reaction mechanism (Fig. 3a) involves the single atom Pt acting as an effective electron receiver, which can accept the photogenerated electrons from SiP and then reduce H^+ to generate H_2, thus realizing the effective isolation of the electron–hole pairs in SiP. In the charge transfer channel (interface charge transfer) mechanism, the interface of SACs-2D material provides abundant active sites, allowing photogenerated carriers to quickly separate at the interface, or single atoms to be inserted between 2D material layers as bridges, thereby accelerating the transport process of photogenerated electrons and holes.

Tong *et al.*[55] doped monoatomic Fe, Co and Ni in g-C_3N_4, respectively, and found that Fe, Co and Ni atoms can be inserted into the interlayers of g-C_3N_4 to act as bridges and improve the charge carrier migration efficiency between the g-C_3N_4 layers. The flow of electrons accumulated on the transition metal into the g-C_3N_4 surface for photocatalytic reactions enhances the interlayer carrier migration and effectively induces the separation of photogenerated electron–hole pairs. In addition, single-atom Fe and Co can form a distinct inherent electric field inside g-C_3N_4, and the inherent electric field accelerates the movement of g-C_3N_4 carriers and generates specific motions of the photo-induced electrons in g-C_3N_4 to promote the separation of carriers in g-C_3N_4. As a result of the combined impact obtained from the inherent electric field

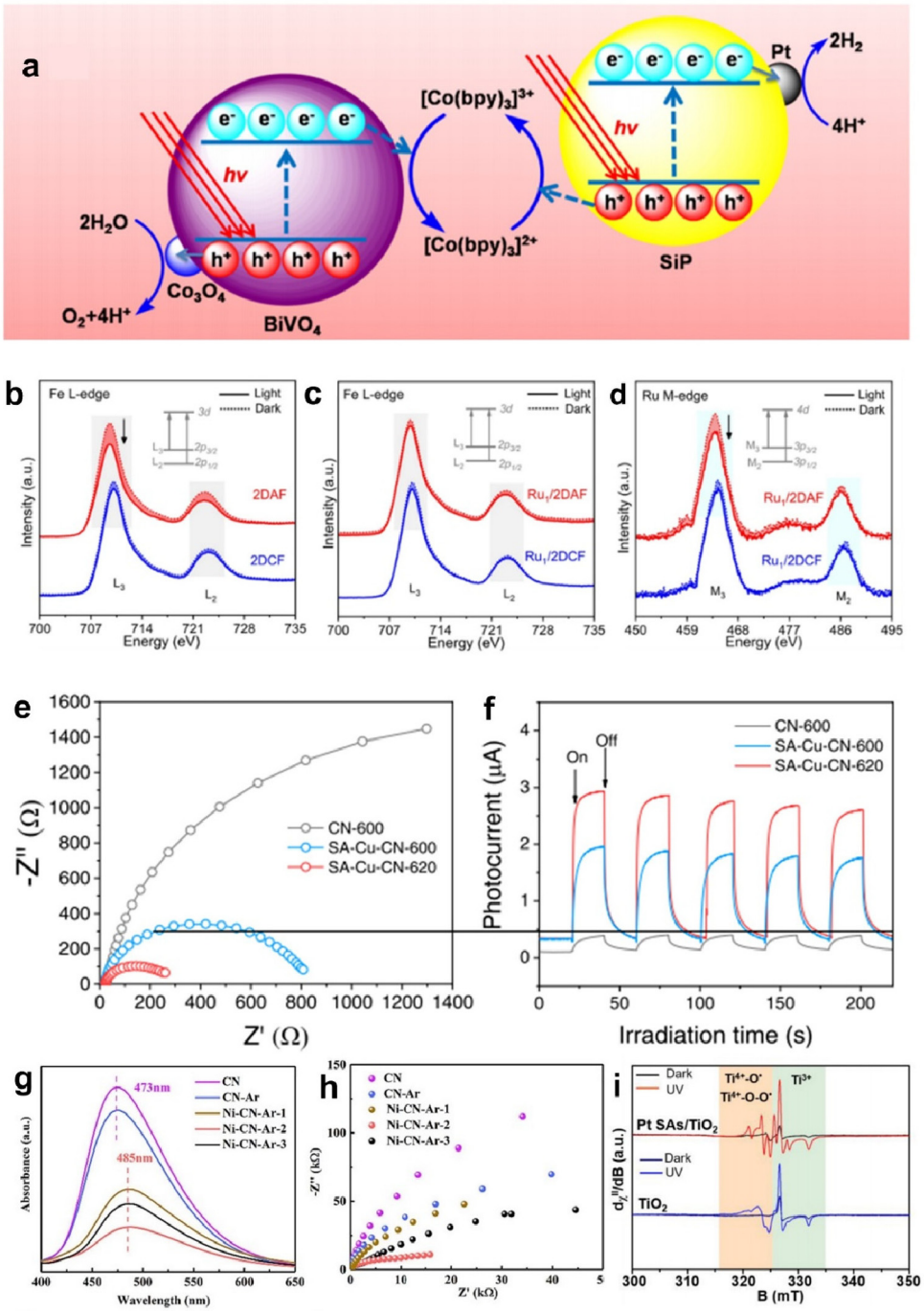

Fig. 3 (a) Reaction mechanism of the Z-scheme Pt/SiP NSs-Co(bpy)$_3^{3+/2+}$-Co_3O_4/$BiVO_4$ system for photocatalytic overall water splitting. Reproduced with permission.[62] Copyright 2022, American Chemical Society. Detection of the electron-transfer process initiated by light. Fe L2,3-edge sXAS of (b) 2DAF and 2DCF in both darkness and illumination, (c) Ru1/2DAF and Ru1/2DCF in both darkness and illumination, (d) Ru M2,3-edge sXAS of Ru1/2DAF and Ru1/2DCF in both darkness and illumination. Reproduced with permission.[63] Copyright 2022, American Chemical Society. (e) Electrochemical impedance spectra, (f) The photocatalytic current response of the catalysts. Reproduced with permission.[64] Copyright 2023, American Chemical Society. (g) Ambient temperature PL spectra excited by 350 nm light, (h) EIS Nyquist plot of the catalysts. Reproduced with permission.[52] Copyright 2024, Elsevier. (i) X-band CW EPR spectra of TiO_2 and Pt SAs/TiO_2 dispersed in H_2O in darkness and UV irradiation. Reproduced with permission.[33] Copyright 2023, American Chemical Society.

of the single-atom Fe and Co atoms/g-C_3N_4 system, the photogenerated electrons aggregated on the surface of g-C_3N_4 can preferentially participate in the photocatalytic reaction instead of being used up through complexation with photogenerated electron–hole pairs, thus contributing to the improvement of the photocatalytic performance of g-C_3N_4. The Chen team[3]

loaded single-atom Pt on TiO_2 and found that the single-atom Pt can not only function as a site for proton reduction, but also enhance the generation of surface oxygen vacancies in adjacent TiO_2. This process results in the development of an atomic interface connecting the single-atom Pt and Ti^{3+} defects, creating an active center with atomically dispersed Pt–O-Ti^{3+}. The photocurrent response graph indicates that Pt1/def-TiO_2 exhibits a higher photocurrent density at the photocathode than f-TiO_2, suggesting that the presence of the distinct Pt–O-Ti^{3+} atomic interface helps to enhance the efficiency of transferring photogenerated electrons from Ti^{3+} defect sites to single-atom Pt, thereby promoting the dissociation of electron–hole pairs and suppressing their subsequent reconstitution. Liu *et al.*[63] investigated single-atom Ru loading on amorphous iron oxide nanosheets for the nitrogen fixation reaction using *in situ* sXAS to observe the changes in the electronic configuration of the photocatalysts during exposure to light. For photocatalysis, when electrons are excited by light, they move from the filled state to the empty state. This means that the increase in electron density in the empty state causes a reduction in the peak of sXAS. Amorphous iron oxide nanosheets (2DAF) showed a large decrease in the peak intensity of the Fe $L_{2,3}$ edge under light compared to crystalline iron oxide nanosheets (2DCF), suggesting that a greater number of photogenerated electrons move to the 3d orbitals of Fe (Fig. 3b). There is a notable reduction in the peak intensity of the Fe $L_{2,3}$ side exposed to illumination when single-atom Ru is loaded on 2DAF (Fig. 3c). It can be seen that the Ru M-edge intensity of Ru_1/2DAF is significantly reduced compared with that of Ru_1/2DCF (Fig. 3d). Therefore, it can be seen that the electronic connection between neighboring Fe and single-atom Ru builds directional channels, accelerates the transmission of light-induced electrons to the Ru active site, and reduces the barrier for electron migration, thus promoting the nitrogen fixation reaction. Shen's team studied Cu-C_3N_4 photocatalytic hydrogen production,[64] SA-Cu-CN showed significantly smaller charge transfer resistance and higher photocurrent compared with CN-600, which demonstrated effective charge separation and transfer through single-atom Cu channels in the C_3N_4 layer to promote photocatalytic hydrogen production, and with this photocatalyst the hydrogen production reached 605.15 μmol g^{-1} h^{-1} (Fig. 3e and f). Under 350 nm excitation, the PL of CN exhibits a prominent emission peak at 473 nm,[52] the emission peak of Ni-CN-Ar-*X* (CN represents g-C_3N_4, and *X* represents the holding time at 550 °C) shifts towards the red end, specifically to 485 nm (Fig. 3g). Ni-CN-Ar-2 exhibits greater photon absorption than CN, and a significant portion of Ni single atom captured photogenerated charges tend to transition into the non-emitting state, leading to a substantial reduction in PL intensity. This phenomenon indicates an effective suppression of charge-carrier complexation. Comparing the EIS plots (Fig. 3h) for the photocatalytic samples, it was observed that the arc radius of the Ni-CN-Ar-2 was the smallest, indicating that the photogenerated carriers had the smallest transfer resistance, and thus the introduction of the single-atom Ni made the carrier separation and transfer efficiency become higher, which improved the photocatalytic activity.

In the study of high-density single-atom Pt loaded on electron-deficient g-C_3N_4,[65] strong reactive metal–support interactions (RMSI) between PtSA and electron-deficient g-C_3N_4 not only improved the stability of PtSA, but also optimised the electron trapping ability and H_2 generation properties of PtSA through electronic and geometrical effects. Based on simulations, it is shown that in the Pt-C_{2C} structure formed by RMSI, there is a strong chemical bond between PtSA and C_{2C} sites, and the C_{2C} sites improve the electron trapping ability of PtSA due to its electron-deficient properties, which facilitates charge-carrier segregation and transport in the photocatalytic process. Wang *et al.*[66] calculated the band gap of Ni/H_xWO_{3-y} hybridization to be 1.28 eV, which is a considerable reduction compared to the band gaps of WO_3 (2.57 eV), Ni/WO_3 (2.50 eV), and H_xWO_{3-y} (1.66 eV), and the introduction of oxygen vacancies and Ni SAs in Ni/H_xWO_{3-y} hybrids improves the photogenerated separation efficiency of electron–hole pairs. Wu's team investigated the stabilization and strongly enhanced photocatalytic hydrogen precipitation performance of fluorine-assisted Pt single atoms on TiO_2 nanosheets.[33] From the EPR maps of TiO_2 as well as Pt-TiO_2 under light illumination (Fig. 3i), it is evident that the presence of Pt SAs on TiO_2 significantly alters the nature of photoexcited electrons and holes. The presence of Pt SAs on titanium dioxide leads to diminished magnetic dipole interactions with proximate spin-effective systems compared to TiO_2, as indicated by sharp signals associated with photoexcited hole centers, indicating that the Pt single atoms in Pt-TiO_2 contribute to the suppression of fast recombination of photogenerated electron–hole pairs. Therefore, the strong interaction between SACs and 2D materials can effectively improve the photocatalytic performance of SACs. This effect is achieved through multiple mechanisms, through which single atom catalysts can optimize the transport of electrons and holes, thereby enhancing the efficiency and selectivity of photocatalytic reactions.

3.3 Accelerated redox kinetics

The surface redox reaction (Fig. 4) usually involves three primary stages: (a) adsorption of reactants on the catalyst surface; (b) transfer of electrons/protons; (c) the structural rearrangement of the product and its desorption from the catalyst surface. The parameters that describe the kinetics of photocatalytic oxidation–reduction mainly include reaction rate constant, quantum efficiency, oxidation–reduction potential as well as adsorption and desorption equilibrium constants. Quantum efficiency refers to the number of molecules involved in a reaction caused by each incident photon. The adsorption and desorption equilibrium constants describe the adsorption capacity of reactants on the catalyst surface and the rate of product desorption from the catalyst surface. Surface redox reactions require reactants to overcome energetic barriers in order to form active intermediate molecules and participate in the conversion of products. However, most of the reactions involve high substrate adsorption activation and

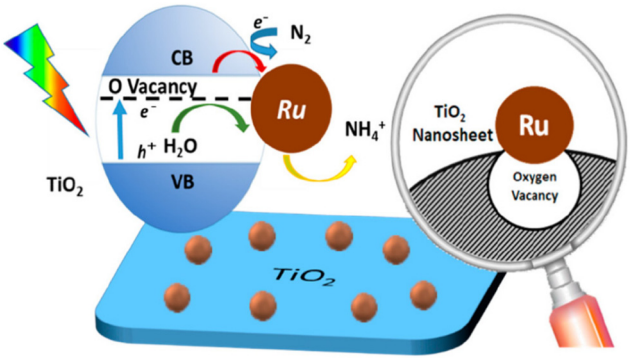

Fig. 4 Example of surface oxidation–reduction diagram. Reproduced with permission.[32] Copyright 2019, American Chemical Society.

product desorption barriers, which severely limit the rate and selectivity of product generation. SCAs-2D can reduce the activation energy barriers at the corresponding stages of the reaction by providing single-atom active sites, modulating the electronic states, and optimizing the formation of intermediates, thus realizing efficient photocatalytic reactions.

Zhang's team[40] used a metal-based ionic liquid induced strategy to uniformly and stably anchor Co metal atoms to the $Bi_{24}O_{31}Br_{10}$ atomic layer, with Co single atoms acting as active sites to accelerate the reaction kinetics. In the study of accelerated photocatalytic hydrogen production by single-atom Pt with high-vacancy d orbitals,[67] it was found that the mutual influence of single-atom Pt with g-C_3N_4 carriers substantially changed the electron distribution of Pt, and its unique electronic structure lowered the kinetic potential barrier, which was conducive to the absorption of hydrogen for the formation of H* and the promotion of hydrogen precipitation reaction. According to XPS (Fig. 5a), the electronic structures of Pt SA/CN and Pt NP/CN were detected, and it was found that Pt SA/CN exhibited lower binding energy at 72.0 eV compared to Pt NP/CN. The smaller the energy barrier that needs to be overcome in the reaction, the higher the reaction rate. The results indicate that the profound interplay between single atom Pt and g-C_3N_4 carrier significantly alters the electronic configur-

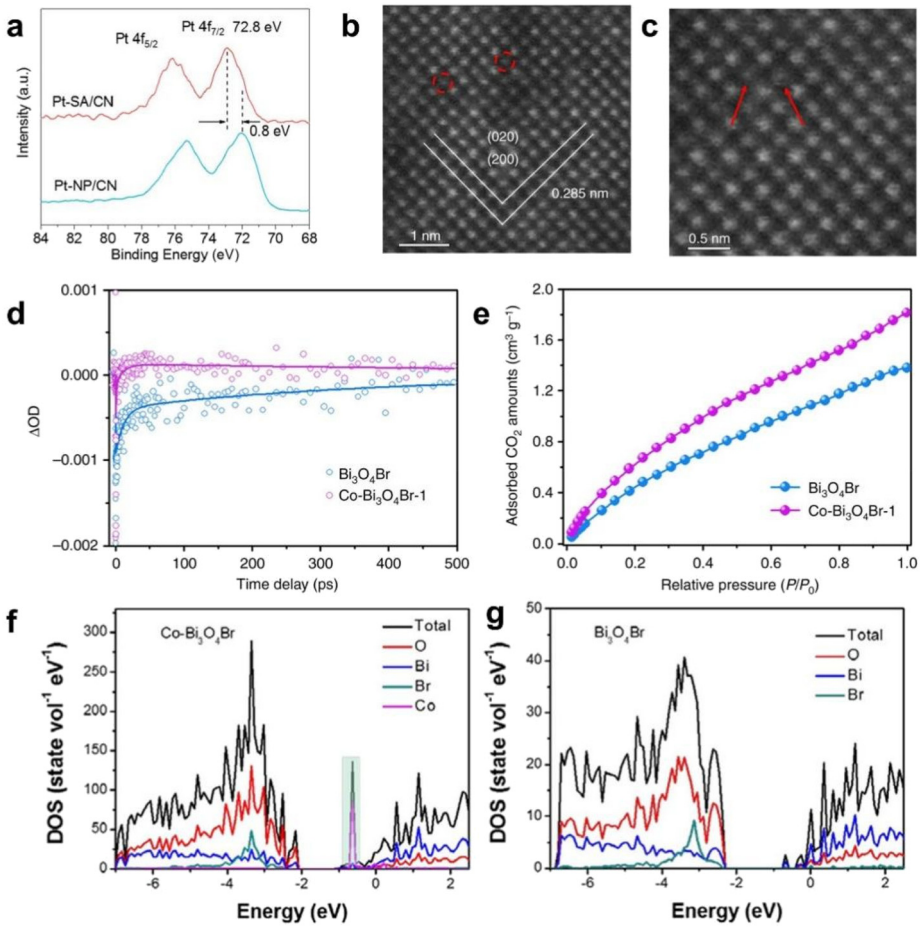

Fig. 5 (a) XPS analysis of the Pt 4f core levels in of Pt-SA/CN and Pt-NP/CN. Reproduced with permission.[67] Copyright 2018, American Chemical Society. (b) and (c) atomic resolution HAADF-STEM images of Co-Bi_3O_4Br-1, (d) ultrafast TA spectra of Bi_3O_4Br and Co-Bi_3O_4Br, (e) CO_2 adsorption isotherms of Bi_3O_4Br and Co-Bi_3O_4Br-1, calculated density of states of (f) Co-Bi_3O_4Br and (g) Bi_3O_4Br. Reproduced with permission.[56] Copyright 2019, Springer Nature.

ation of single atom Pt. The introduction of Co monomers promotes the activation of CO_2, stabilizes reaction intermediates, and reduces the activation energy barrier of the rate limiting step, which is beneficial for improving photocatalytic performance. Taking single atom Co doped Bi_3O_4Br as an example,[56] HAADF-STEM (Fig. 5b and c) shows that Co SAs replace Bi atoms in the lattice, the COOH* intermediate can be stabilized to reduce the activation energy barrier of carbon dioxide, and the rate-controlling step can be adjusted based on the creation of the adsorption intermediate COOH* to CO* desorption, thereby improving the reduction of CO_2 (Fig. 5d and e). Co-Bi_3O_4Br exhibits excellent performance in converting CO_2 to CO, achieving an impressive generation of up to 107.1 μmol g^{-1} h^{-1}, which is 4 times and 32 times higher than the atomic layer and bulk Bi_3O_4Br, respectively. Introducing single atom Pt in combination with C_3N_4, the Pt-N_4 ligand active site facilitates the generation of *COOH intermediates, lowers the reaction potential barrier, reduces the CO_2 activation energy, and improves CO_2 reduction activity and CO selectivity.[50]In the study of single atom Mo loaded on PCN for photocatalytic nitrogen fixation,[22] there is only physical adsorption between PCN and N_2 molecules, while there is robust chemical adsorption between the Mo center of Mo-PCN and N_2 molecules. The formation of Mo–N≡N with the substrate initiated by a single atom. Its strong interaction causes an increase in the distance between the two N atoms in the adsorbed N_2 molecule, exhibiting a decrease in the bonding energy of N≡N, which will contribute to the breakage of the N≡N bond and its conversion to NH_3. For the Au/$ZnIn_2S_4$ catalyst,[39] the low-coordinated and charge-enriched single-atom Au serves as the active site, which effectively reduces the activation energy barrier of CO_2 molecules and thus facilitates CO_2 reduction. Detailed characterization and density functional theory calculations show that Au/$ZnIn_2S_4$ not only exhibits fast carrier transfer, but also reduces the energy barrier for *CO protonation and stabilizes the *CH_3, which results in the selective production of CH_4 by CO_2 photoreduction (Fig. 6a–c). Pt-TiO_2 photocatalysts[46] for hydrogen production can improve the performance of photocatalytic hydrogen precipitation by reducing the H* adsorption energy through the introduction of monoatomic Pt. Wang and colleagues[68] doped Pd into CeO_2 nanosheets, and Gibbs free energy calculations showed that the introduction of single atom Pd greatly reduced the energy barrier for H_2O oxidation, lowered the energy barrier for the formation of intermediates CO* and CH_3O*, and thus promoted the process of CO_2 reduction to CH_4. Long *et al.*[69] reported that Pd_7Cu_1-TiO_2 was used for the photocatalytic CO_2 reduction for the preparation of CH_4. Trace amounts of monatomic Cu were doped into the Pd lattice to form paired Cu–Pd sites, which enhanced the d-band centers of the Cu sites and enhanced the adsorption of CO_2, thereby accelerating the rate of the redox reaction. Xiong *et al.*[70] revealed the unique function of single atom Ni in the extremely selective conversion of biomass byproducts into high-value chemicals using Ni-TiO_2 photocatalysis. The introduction of Ni single atom can effectively enhance the adsorption of oxygen, act as an electron trap, expedite the generation

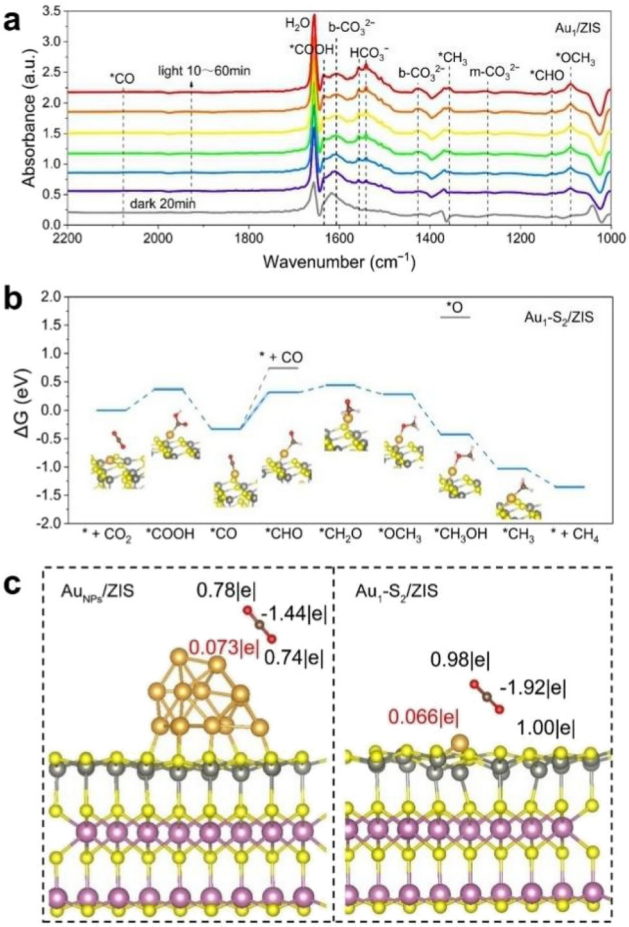

Fig. 6 (a) Detecting intermediates in reactions *via in situ* DRIFTS, (b) free energy diagram for the conversion of CO_2 to CH_4, (c) the optimized adsorption arrangements of CO_2 molecules with their associated charge distribution on the surface of AuNPs/ZIS and Au1-S2/ZIS. Reproduced with permission.[39] Copyright 2022, Wiley-VCH.

of superoxide radicals, and thus improve the selectivity for ethanol aldehyde. Through these studies, it can be seen that SACs-2D catalyst has great potential in photocatalytic reactions. SACs-2D materials significantly reduce the activation energy of the reaction by providing efficient active sites, enhancing the selectivity and stability of the reaction.

4. Photocatalytic applications

The applications of SACs-2D materials in photocatalytic water splitting,[71–73] the reduction of carbon dioxide,[74–76] decomposition of organic contaminants,[77] nitrogen fixation[78] and photocatalytic production of hydrogen peroxide[79] have been widely studied. Despite the promising potential of these applications, they are confronted with substantial challenges, including limitations in redox potential, activation methods of substrates, and stability of catalysts. More specifically, the decomposition of water requires overcoming the high surface

tension of water and the binding energy between water molecules. By loading 2D materials with single atoms on the surface, the valence/conduction band positions of the material can be regulated to meet thermodynamic requirements, thereby reducing the energy required for water electrolysis and improving reaction efficiency. In the realm of CO_2 reduction, the process involves multiple electron and proton transfer steps, each with a different redox potential. The diversity of products resulting from CO_2 reduction further complicates the matter, as controlling product selectivity presents a significant challenge. Loading single atom catalysts on the surface of 2D materials can promote the transfer of electrons and protons, reduce the reaction energy barrier, and improve the efficiency and product selectivity of CO_2 reduction. Furthermore, the degradation of organic pollutants, which exhibit complex mechanisms and diverse structures, requires highly selective catalysts to target specific contaminants. The surface loading of single atom catalysts on 2D materials can improve their adsorption and degradation capabilities for specific organic pollutants by regulating their surface properties and active site density. In the context of photocatalytic nitrogen fixation, the high bond energy of the N≡N triple bond poses a considerable obstacle to its activation at ambient temperatures. SACs-2D materials can effectively promote the cleavage of these bonds by enhancing the adsorption and activation of nitrogen gas, thereby optimizing the reaction pathway and reducing the energy barrier associated with nitrogen fixation. Lastly, the synthesis of hydrogen peroxide requires a delicate balance between selectivity, purity, and yield, while managing oxygen's high reducibility. SACs-2D structure can regulate the reaction pathway to improve the selectivity and yield of H_2O_2, while simultaneously minimizing the formation of by-products. Overall, the SACs-2D structure can effectively regulate the key steps and pathways in photocatalytic reactions, improve reaction efficiency and selectivity, and thus promote the development of these important applications.

4.1 Photocatalytic water splitting

The utilization of solar energy to produce clean fuel hydrogen is seen as a potential approach to mitigate the escalating issues related to energy and environmental pollution stemming from the burning of fossil fuels.[80] As a sustainable hydrogen production method, photocatalytic water splitting has been extensively researched in recent decades.[81] The water splitting process involves complex photochemical reactions, especially in artificial photocatalytic systems. The following is the general pathway reaction equation for photocatalytic water splitting, which is divided into two main half reactions:

Direct photocatalytic pathway:

$$2H_2O \rightarrow O_2 + 4H^+ + 4e^-$$

$$4H^+ + 4e^- \rightarrow 2H_2$$

Photon generated holes participate in the pathway:

$$2h^+ + H_2O \rightarrow 1/2O_2 + 2H^+$$

$$2e^- + 2H^+ \rightarrow H_2$$

There are many reasons for the low efficiency of photocatalysts, including but not limited to insufficient light absorption capacity, rapid electron–hole pair complexation, insufficient surface active sites, diffusion limitation of the reactants, and occurrence of side reactions. Loading single atoms not only captures electrons, but also provides effective proton reduction sites, significantly improving photocatalytic performance, which is an efficient method for inhibiting photogenerated electron–hole pair recombination. For example, single atom Pt is anchored on g-C_3N_4 with high dispersibility and stability, achieving maximum utilization of Pt atoms. Single atom Pt induces intrinsic changes in surface trap states, thereby extending the lifetime of photogenerated electrons and significantly improving photocatalytic hydrogen evolution activity.[82] In the process of photocatalytic water splitting, light stimulates the charge transfer on the surface of the luminescent catalyst, decomposing water molecules into oxygen and hydrogen gas.[83] SACs-2D material catalysts have a large specific surface area, excellent carrier transport characteristics, and flexible surface regulation ability, making them ideal photocatalysts.

Many studies have been conducted by combining single atoms with 2D materials, and the main single atoms used are precious metals (Au, Pt, Rh, Pd, *etc.*), transition metals (Fe, Co, Ni, Cu, *etc.*) and rare earth metals, ascribed to their rich valence states, diverse coordination environments, and controllability. Single-atom Pt^{II} was stabilized on the surface of g-C_3N_4,[23] and the examination of the photocatalytic water splitting activity of the photocatalysts revealed that in pure water photocatalytic measurements (Fig. 7a), there was virtually no production of H_2 from g-C_3N_4, and a small quantity of H_2 was observed from Pt NP-C_3N_4, whereas the rate of H_2 gas production from Pt^{II}-C_3N_4 was as high as 140 μmol g^{-1} h^{-1}, which is about 10 times higher than that of Pt NP-C_3N_4 (15 μmol g^{-1} h^{-1}). This implies that Pt^{II} loaded onto the surface of g-C_3N_4 promotes the oxidation of water, which splits water for efficient hydrogen production. Further calculations and electrochemical characterization (Fig. 7b) showed that Pt^{II} bound to g-C_3N_4 could decrease the VBM level by 0.26 V with respect to g-C_3N_4, which promoted the kinetics of the water oxidation reaction for direct photocatalytic water decomposition. These studies show that anchored single atoms can serve as active sites for photocatalytic reactions, as well as change the light absorption process and energy band structure. Moreover, single atom Pt is designed to load on electron deficient g-C_3N_4 for hydrogen production through water splitting, and the calculated hydrogen production mass activity of PtSA-CN620 (174.5 mmol g^{-1} h^{-1}) is 8 times higher than that of PtNP-CN620 (20.5 mmol g^{-1} h^{-1}). Research has shown that the reactive metal–support interaction (RMSI) between single atom Pt and g-C_3N_4 helps to form high-density Pt SAs (0.35 mg m^{-2}) on electron-poor g-C_3N_4, demonstrating enhanced photocatalytic ability to generate H_2. Cao *et al.*[67] reported that Pt-C_3N_4 photocatalytic hydrogen production exhibited a hydrogen

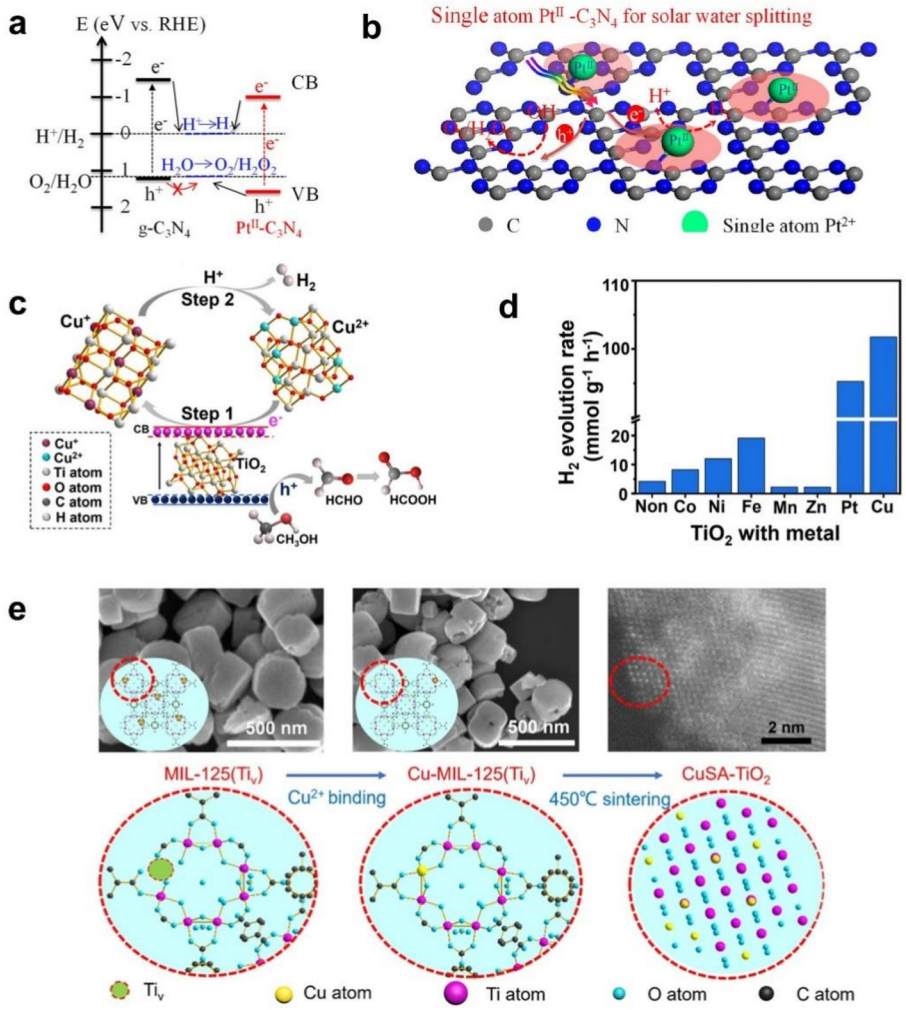

Fig. 7 (a) Band structure alignment schematic for g-C_3N_4 and Pt^{II}-C_3N_4, (b) Schematic representation of the Pt^{II}-C_3N_4 photocatalytic water splitting. Reproduced with permission.[23] Copyright 2018, American Chemical Society. (c) The process of photocatalytic H_2 evolution *via* CuSA-TiO_2, (d) The photocatalytic efficiency in generating H_2 for TiO_2 and M-TiO_2, (e) The diagrammatic depiction of how Cu SAC is formed within the Ti lattice structure of TiO_2. Reproduced with permission.[84] Copyright 2022, Springer Nature.

production rate of 42.1 for Pt-SA/CN μmol h^{-1}, which is 1.7 times (24.4) higher than Pt NP/CN μmol h^{-1}, and the turnover rates (TOF) of Pt SA/CN and Pt NP/CN were 250 and 19.5 h^{-1}, respectively. Li *et al.*[82] generated H_2 through Pt/g-C_3N_4 photocatalytic water splitting, and the improvement in photocatalytic H_2 generation efficiency is attributed to the intrinsic changes in the introduction of single atom Pt into the surface trap state of g-C_3N_4. The above results indicate that Pt-C_3N_4 has high performance in water splitting hydrogen production applications. Zhang *et al.*[84] achieved a widely scattered and substantial amount (>1wt%) of SA Cu on TiO_2 in a water cracking hydrogen production study (Fig. 7c), and the hydrogen evolution rate of Cu-TiO_2 was as high as 101.7 mmol g^{-1} h^{-1} (Fig. 7d) under illumination, which was higher than that of other photocatalysts that have been recorded and demonstrated excellent stability after storage for 380 days. The creation of Cu single atoms in the titanium lattice of TiO_2 (Fig. 7e) also represents a significant advancement in this area with a recorded quantum efficiency of 56% at 365 nm. Single atom Pt is designed to load on electron deficient g-C_3N_4 for hydrogen production through water splitting,[65] and the calculated hydrogen production mass activity of PtSA-CN620 (174.5 mmol g^{-1} h^{-1}) is 8 times higher than that of PtNP-CN620 (20.5 mmol g^{-1} h^{-1}). Sun *et al.*[26] prepared a Ce-SA-C_3N_4 catalyst composed of rare earth single atom Ce on C_3N_4 nanosheets (Fig. 8). According to X-ray absorption spectroscopy (XAS) and density functional theory (DFT) calculations, single atom Ce is coordinated by 4 N atoms and 6 O atoms (Ce-N_4/O_6), which serve as active sites and facilitate the transfer and separation of charges. The Ce-SA-C_3N_4 photocatalyst was utilized to decompose water into hydrogen gas, achieving a peak hydrogen gas production of 33.5 mmol h^{-1} g^{-1}. At 420 nm, the apparent quantum efficiency of hydrogen production reaches 32.6%. The performance of SACs-2D photocatalysts has been significantly enhanced, which provides a more effective way for clean hydrogen production and

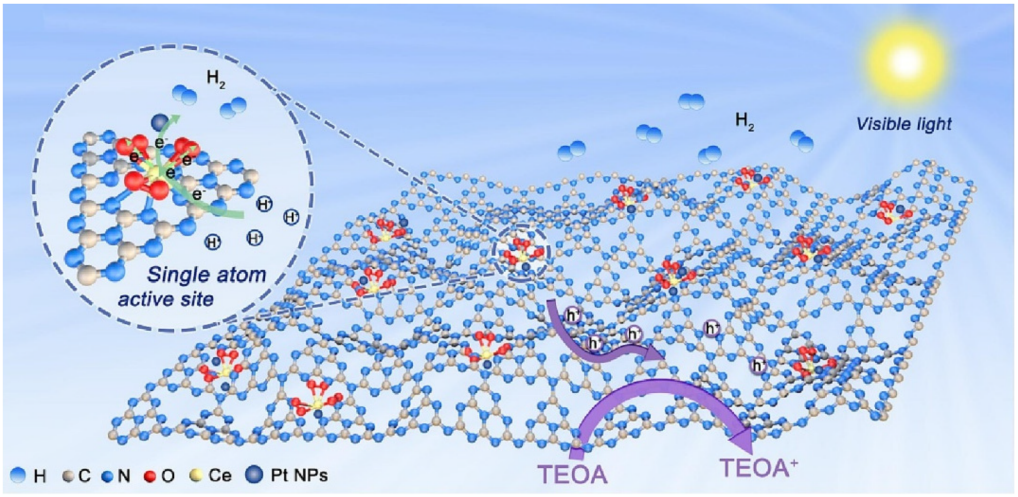

Fig. 8 The illustrative representation of the photocatalytic hydrogen generation process in Ce-SA-C_3N_4. Reproduced with permission.[26] Copyright 2023, Elsevier.

contributes to the development of environmentally friendly energy technologies.

4.2 Photocatalytic reduction of carbon dioxide

Global energy consumption continues to increase over time due to advances in social living standards and industrialization, and over-reliance on non-sustainable fossil fuels exacerbates the consumption of finite resources while generating large quantities of CO_2, which is the primary source of global warming.[85] Photocatalytic reduction, which converts CO_2 into value-added chemical fuels through imitation of the natural photosynthetic procedure, offers a viable pathway to solve the escalating CO_2 emissions and the severe energy crunch. CO_2 reduction reactions are highly challenging because the CO_2 molecule itself is very stable and needs to overcome a large activation energy to convert it into other compounds.[86] In this area of research, it is important to consider not only the selectivity and efficiency of the reaction, but also its sustainability, economics, and feasibility for practical applications. The reaction pathways corresponding to different CO_2 reduction products are different, and the proton coupled electron transfer processes involved are also different. For instance, during the reduction of CO_2 to CO, the initial step involves the adsorption of CO_2 molecules onto the catalyst surface, followed by an electron transfer that reduces the CO_2 molecules to $CO_2^{\bullet-}$ intermediates. Subsequently, these intermediates undergo a second electron transfer, desorbing from the catalyst surface to form $CO_2^{\bullet-}$ intermediates. The final reduction step releases CO gas, regenerating the active catalyst surface. While in the case of CO_2 reduction to produce CH_3COOH,[59] the proton-coupled electron transfer process initiates with CO_2 accepting six protons (H^+) and six electrons (e^-), resulting in the formation of CH_3CHO and two water molecules. In the subsequent step, CH_3CHO is transformed into CH_3COOH through the action of water, with the release of two protons and two electrons. These intricate processes underscore the need for precise control and optimization in the design of catalysts for CO_2 reduction reactions.

Huang *et al.*[45] reported utilizing Co^{2+}-C_3N_4 for the reduction of CO_2 and showed that bare C_3N_4 resulted in an imperceptible amount of CO production, and that a notable quantity of CO was produced when a combination of $CoCl_2$ and C_3N_4 was used for CO_2 reduction. However, at an equivalent cobalt concentration, the CO production of Co^{2+}-C_3N_4 was approximately five times greater than that of the combination of $CoCl_2$ and C_3N_4, and single atom Co^{2+} contributes significantly to CO_2 reduction. As the cobalt loading goes up, the amount of CO generated during CO_2 reduction increases proportionally. Photocatalytic and spectroscopic investigations unequivocally establish the presence of isolated Co^{2+} sites and their pivotal significance in attaining selective CO_2 reduction. The introduction of single atom Co^{2+} results in a quantum yield of up to 0.40% for CO production. Gao *et al.*[87] fixed Co on partially oxidized graphene nanosheets through heat treatment in their study for CO_2 reduction to CO (Fig. 9a). The author compared pure graphene nanosheets and Co loaded graphite nanosheets (named G and Co-G, respectively). Thanks to the stability effect of the two-dimensional support and the interaction between Co atoms and the support, Co-G exhibited excellent catalytic performance (TON generated by CO in the first 3 hours was 374, TOF was 2.08 min^{-1}) and high selectivity for CO (79.4%) (Fig. 9b). Si *et al.*[39] achieved excellent photocatalytic CO_2 reduction performance by loading single-atom Au on ultrathin $ZnIn_2S_4$ nanosheets *via* the complex exchange pathway (Fig. 9c). Upon exposure to visible light, the Au-$ZnIn_2S_4$ catalyst exhibited a CH_4 production of 275 μmol g^{-1} h^{-1} with a selectivity of 77%. In the CO_2 reduction reaction, converting CO_2 molecules into C1 products such as CO, HCOOH, or CH_4 requires different numbers of electrons to participate (Fig. 9d). In particular, for the conversion to CH_4, this process requires the most electron transfer (8 electrons), so the conversion of CO_2 to CH_4 is one of the most challenging

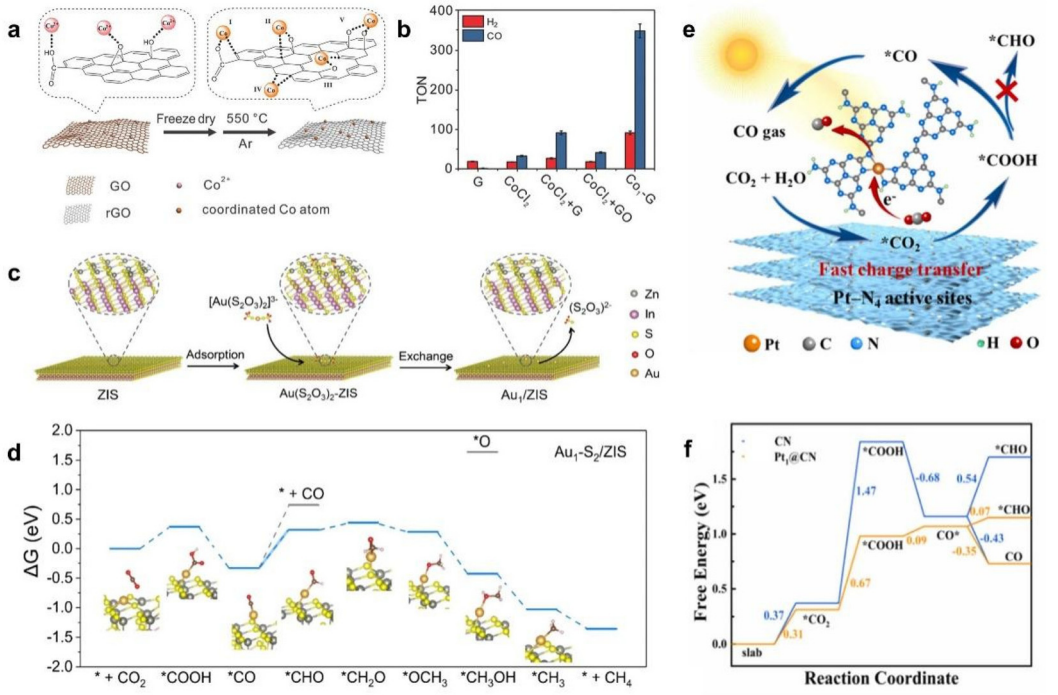

Fig. 9 (a) Diagrammatic overview of the Co1-G catalyst's synthesis, (b) TONs of H_2 and CO production across various catalysts. Reproduced with permission.[87] Copyright 2018, Wiley-VCH. (c) Schematic illustration for the preparation of Au_1/ZIS by a complex-exchange route, (d) free energy profile of CO_2 Reduction on Au_1-S_2/ZIS catalysts. Reproduced with permission.[39] Copyright 2022, Wiley-VCH. (e) Mechanism of CO_2 reduction on Pt-N_4 active sites under solar illumination, (f) free energy diagram for CO_2 reduction on CN and Pt1@CN catalysts. Reproduced with permission.[50] Copyright 2024, Elsevier.

tasks in CO_2 reduction reactions. The alloying method[69] was used to load the isolated Cu atoms in the Pd lattice over a TiO_2 support for CO_2 photocatalytic conversion to CH_4, the findings indicated that the selectivity of Pd_7Cu_1-TiO_2 photocatalyst for CH_4 was 96%, and the reaction rate was 19.6% μmol g_{cat}^{-1} h^{-1}. Hu *et al.*[50] reported a stable and productive photoreduction of CO_2 by a single-atom Pt-anchored porous C_3N_4 nanosheet photocatalyst (Pt_1-CN) coordinated with Pt-N_4 (Fig. 9e). The reaction rate of Pt_1-CN was 84.8 μmol g^{-1} h^{-1}, and the CO selectivity was close to 100%, practically 100% CO-specificity is possibly the result of the quick eviction of *CO groups, allowing for the creation of CO molecules on Pt (Fig. 9f), which was superior to that of most of the C_3N_4-based single-atom photocatalysts. Ding and his colleagues[88] synthesized Pd Co_3O_4 to photocatalytically reduce CO_2 to CH_3COOH. The introduction of a single atom Pd leads to a charge asymmetric Co *para* site. Calculations show that the charge asymmetric Co *para* site reduces the reaction potential barrier of the rate limiting step, which lowers the formation energy barrier of C–C coupling, thereby promoting the conversion of CO_2 to CH_3COOH. Different SACs-2D photocatalysts produce different products with high selectivity in the CO_2 reduction reaction, such as CO and CH_4, the selectivity of CO_2 reduction varies depending on the type of single atom, for example, the CO selectivity of Cu/g-C_3N_4 is close to 100%;[89] the CO selectivity of Pt/g-C_3N_4 is nearly 100%;[50] the CO selectivity of Co/g-C_3N_4 is about 87%, and the CH_4 selectivity is about 13%;[61] The CH_4 selectivity of Au/$ZnIn_2S_4$ is as high as 77%.[39] Consequently, future studies may focus on modulating the type of single atom to optimize the selectivity for the desired product. However, whether converting CO_2 into CO, CH_4, or CH_3COOH, they all convert CO_2 into valuable chemical fuels, which can be used to solve the problem of increasing CO_2 emissions and to cope with the energy crisis.

4.3 Photocatalytic degradation of organic pollutants

There are various types of organic pollutants present in the environment, such as dyes, antibiotics and pesticides. Dye-based pollutants include methylene blue in cosmetics and rhodamine B used in the garment industry; antibiotic-based pollutants include sulphonamides and tetracyclines; and pesticide-based pollutants include benzene, preservatives and bisphenol-A. These organic pollutants not only cause serious damage to the ecological environment, but also pose unpredictable risks to human health. Due to its bioaccumulation and environmental persistence, it can be absorbed and accumulated in human organs, thereby posing adverse impacts on human health. These include, but are not limited to, provoking immune system alterations, endocrine imbalances, pregnancy complications such as miscarriage, and carcinogenicity.[90] Consequently, developing appropriate methods for mineralization and degradation of organic pollutants is a key challenge in treating organic pollutants in wastewater.[91] In the degradation of

organic pollutants, SACs-2D photocatalytic materials can use visible or ultraviolet radiation to excite electrons and produce active oxides. These products have strong oxidation ability and can directly react with organic pollutants, degrading them into harmless substances such as water and carbon dioxide.

The Wang's team[25] prepared a single atom dispersed Ag-doped mesoporous graphitic carbon nitride (Ag/mpg-C_3N_4) photocatalysts for the degradation of bisphenol A (BPA) using the co-condensation method (Fig. 10a). In the study, it was found that the elimination of BPA increased from 88% to 99.4% when the monoatomic Ag content was increased from 1% to 10%. The diffuse reflectance UV-visible spectra of Ag/mpg-C_3N_4 with different Ag contents showed that the thresholds for visible absorption shifted towards longer wavelengths with increasing Ag content. This shift corresponds to the narrowing of the optical band gap, thus enhancing the excitation process. Meanwhile, the photocurrent was significantly enhanced by the introduction of monoatomic Ag, indicating that the introduction of Ag effectively inhibited the complexation of light-induced electron–hole pairs, consequently favoring the degradation of BPA. Zhang *et al.*[92] synthesized Ce-doped Bi_2WO_6 (Ce-Bi_2WO_6) nanosheets enriched with oxygen vacancies using a simple hydrothermal method (Fig. 10b). The Ce-Bi_2WO_6 catalysts were enriched with oxygen deficiencies, and the bandgap underwent a reduction from 2.78 eV (Bi_2WO_6) to 1.61 eV, which contributed to the improvement of photocatalytic activity. Because of the creation of oxygen vacancies, the nanosheets exhibited higher photocatalytic efficiency with a TCH degradation rate of 61.1% in 40 min. In addition, the inclusion of H_2O_2 can further improve the TCH decomposition rate through the Fenton reaction, achieving a removal efficiency of 90.4%, thus demonstrating a powerful synergistic action between oxygen vacancies and H_2O_2 in Ce-Bi_2WO_6. Covalent triazine frameworks (CTFs)[93] are 2D porous materials with a π-conjugated structure, and the triazine unit can potentially evolve into a bifunctional material, capable of adsorption as well as photocatalysis. Zhu *et al.* anchored single-atom Ti to structurally well-defined N-rich CTFs (named Ti-CTFs). The study used a mild two-step method to introduce single-atom Ti into the pristine CTF, which dramatically changed the electronic configuration and spin state of the active site. The spin-polarized Ti-N_3 groups facilitated the treatment of organic pollutants (especially those in natural water) through the intensification of induced dipole adsorption and the expedited production of O_2^- during the photocatalytic process. When contrasted with other sophisticated oxidation processes (*e.g.*, UV/periodate oxidation, ozone oxidation, and electro-oxidation), Ti-CTF exhibited a high adsorption (453.285 μmol g^{-1}) and photocatalytic rate (2.263 h^{-1}) using only sunlight exposure (Fig. 10c). As stated above, the combination of single-atom noble metals and 2D materials is capable of significantly elevating the rate of photocatalytic degradation by changing the electronic structure and surface active sites of the materials to achieve efficient degradation and removal of organic pollutants, and the design of suitable photocatalysts is crucial for the treatment of organic pollutants.

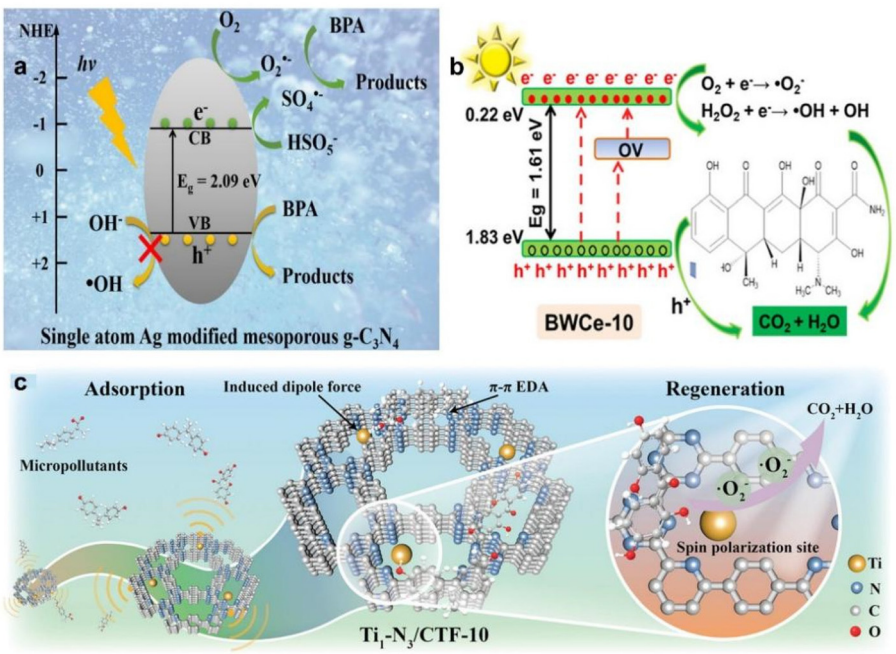

Fig. 10 (a) Schematic of photocatalytic degradation pathway on single atom Ag-modified mesoporous g-C_3N_4. Reproduced with permission.[25] Copyright 2017, Elsevier. (b) photocatalytic mechanism of the BWCe-10 photocatalyst for TCH degradation. Reproduced with permission.[92] Copyright 2024, American Chemical Society. (c) Schematic diagram of the mechanism for removing pollutants. Reproduced with permission.[93] Copyright 2023, Wiley-VCH.

4.4 Photocatalytic nitrogen fixation

Nitrogen fixation refers to the chemical transformation of atmospheric nitrogen into ammonia or other organic compounds, and is an important industrial method. Traditional nitrogen fixation reactions (Haber–Bosch process) usually require the use of metals such as iron and molybdenum as catalysts under high temperature and high pressure conditions, but these methods suffer from high energy consumption, poor product selectivity, and complex equipment. The industrial production of NH_3 is highly energy intensive, consuming large amounts of fossil fuels and emitting large amounts of carbon dioxide.[94] The nitrogen reduction directly driven by solar energy represents a method of synthesizing ammonia with water under mild conditions, which has great hope in reducing energy consumption and alleviating environmental challenges caused by traditional processes. Nitrogen reduction has three different reaction mechanisms (Fig. 11a–c): dissociation, alternate binding and distal binding pathways.[95] In the dissociation mechanism,[96] the N≡N of the N_2 molecule is the first to break, followed by hydrogenation to eventually form NH_3 (Fig. 11a). However, direct nitrogen reduction is a very challenging reaction both kinetically and thermodynamically. In both the alternating and distal association pathways, the N_2 molecule is first hydrogenated, followed by the breaking of the N≡N bond, and finally the formation of NH_3. The difference is that in the alternating association pathway, the proton addition occurs either directly or indirectly close to the N (Fig. 11b); in the distal association pathway, the addition of protons occurs away from the surface of the catalyst (Fig. 11c).

Interaction between monatomic Ru and the second coordination sphere for efficient nitrogen fixation,[97] research has found that when Ru single atom is loaded on CoO, there is a strong interaction between Ru and the second coordination sphere (Co atom in CoO), and additional Ru–Co coordination is observed. Ru–Co coordination acts as an additional photoelectron transfer channel, promoting the excitation and accumulation of photoelectrons from O atom to Co atom and then to Ru active site, thereby accelerating the process of N_2 photoreduction to NH_3 (Fig. 11d). For N_2 photoimmobilization, the ammonia production rate of Ru_{O+Co}/CoO was 306 μmol $gcat^{-1}$ h^{-1}, which was 4.6 times higher than that of Ru_O/CoO. Ling *et al.*[21] proposed using a non-metallic single atom, namely, boron atom, to modify the optical activity of g-C_3N_4 to facilitate the reduction of N_2. In the immobilized B single atom, the N_2 charge transfer is bidirectional, and charge buildup and exhaustion could be detected in both the N_2 molecule and the B atoms, *i.e.*, the single atom B accepts lone-pair electrons, while giving electrons to the antibonding electronic states of N_2. These calculations confirmed a high bond strength as well as bidirectional charge exchange between N_2 and B/g-C_3N_4. It was found that with the modification of the B atom, the band gap was reduced to 1.12 eV, which resulted in enhanced visible and infrared light acquisition and good nitrogen fixation activity of B/g-C_3N_4 (Fig. 11e). Guo *et al.*[22] used Mo monoatomic loading on PCN for N_2 reduction to NH_3 and demonstrated that with the rise in Mo content, the activity of Mo-PCN also rises, as well as the highest yield of NH_3. Di and colleagues[37] used atomic layer constrained doping to prepare Cu-$Bi_{24}O_{31}Br_{10}$ for nitrogen fixation. The experiment found that Cu-Bi sites formed surface

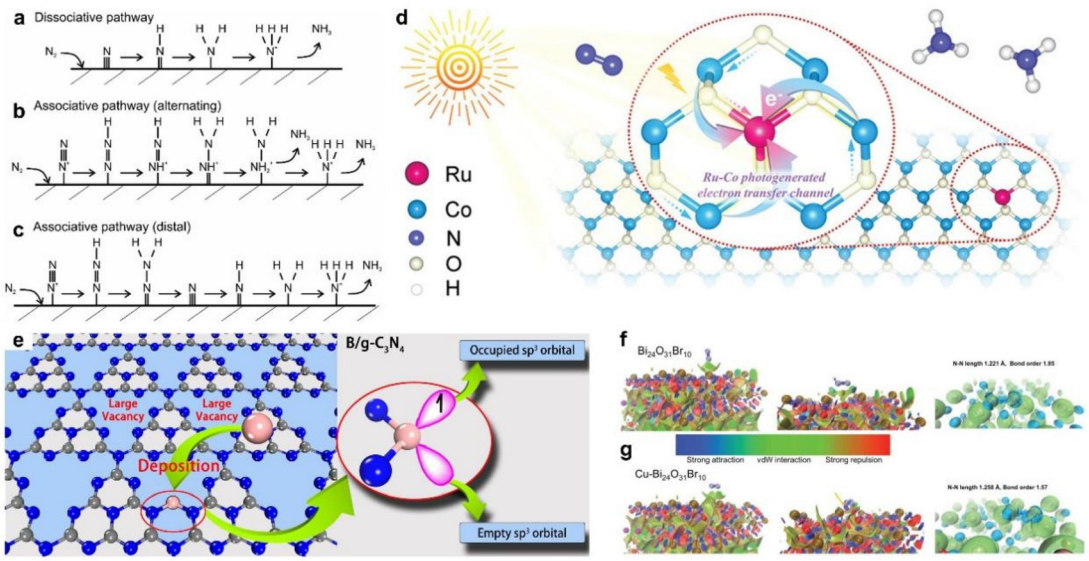

Fig. 11 Three mechanisms of nitrogen reduction: (a) dissociation, (b) alternate binding, (c) distal binding pathways. Reproduced with permission.[95] Copyright 2014, Royal Society of Chemistry. (d) Schematic illustration of N_2 photofixation reaction mechanism over Ru-CoO. Reproduced with permission.[97] Copyright 2022, Wiley-VCH. (e) Design concept of as a photocatalyst for N_2 fixation using B/g-C_3N_4. Reproduced with permission.[21] Copyright 2018, American Chemical Society. (f) Isosurface maps of IRI = 1.0 between N_2 and $Bi_{24}O_{31}Br_{10}$, *NNH and $Bi_{24}O_{31}Br_{10}$, (g) Isosurface maps of IRI = 1.0 between N_2 and Cu-$Bi_{24}O_{31}Br_{10}$, *NNH and Cu-$Bi_{24}O_{31}Br_{10}$ Reproduced with permission.[37] Copyright 2022, Wiley-VCH.

local polarization around them, providing a local electric field to accelerate carrier separation and improve the conversion of N_2 to NH_3 (Fig. 11f and g). The combination of single atoms and two-dimensional materials promotes N_2 reduction through metal carrier interactions, selective nitrogen reduction driven by bimetallic sites, formation of heterojunctions or additional charge transfer channels. During nitrogen fixation, the combination of single atoms and 2D materials can effectively promote the conversion of intermediates, reduce the activation energy of the reaction, and accelerate the process of nitrogen reduction to ammonia. Through the analytical review of the various methodologies employed by different research teams and the outcomes of photocatalytic nitrogen fixation using diverse materials, it becomes evident that the amalgamation of single atoms with two-dimensional materials offers novel strategies for photocatalytic nitrogen fixation. This synergy holds great potential for mitigating energy consumption and addressing pressing environmental challenges.

4.5 Photocatalytic production of hydrogen peroxide

Hydrogen oxide (H_2O_2) is a vital oxidizing and disinfecting agent with extensive applicability in the domains of medicine, food, and environment. The conventional anthraquinone process for extensive industrial-scale production of H_2O_2 suffers from severe shortcomings such as intensive energy utilization, significant waste accumulation, and toxic side product. The synthesis of H_2O_2 by photocatalytic synthesis of H_2O and O_2 using solar-driven semiconductor catalysts is a green, economic and viable approach for H_2O_2 production. There are multiple pathways for photocatalytic reactions to generate H_2O_2.

Direct photoreduction pathway:

$$2H_2O + 2e^- \rightarrow H_2 + H_2O_2$$

Indirect photoreduction pathway:

$$O_2 + 2e^- \rightarrow O_2^{\bullet -}$$

$$O_2^{\bullet -} + H_2O \rightarrow HO_2^{\bullet} + OH^-$$

$$HO_2^{\bullet} + e^- \rightarrow H_2O_2$$

Photon generated holes participate in the path:

$$H_2O \rightarrow {}^{\bullet}OH + H^+ + e^-$$

$$2 \cdot OH \rightarrow H_2O_2 + H_2O$$

The research conducted by Zhang *et al.*[20] has introduced the utilization of monoatomic nickel (Ni) integrated with the two-dimensional material graphitic carbon nitride (g-C_3N_4) for the synthesis of hydrogen peroxide (H_2O_2). The Ni single atoms optimize the electronic structure of the catalyst and enhance the selectivity towards oxygen (O_2), facilitating the production of hydroxyl radicals ($^{\bullet}OOH$). Fig. 12a shows the transformation process: Ni–N_3 → O_1–Ni–N_2 → HOO–Ni–N_2. Among them, the structure of the O_1–Ni–N_2 intermediate state not only inhibits the dissociation of O_2 and improves the selectivity, but also promotes the conversion of the intermediate state to H_2O_2, thus improving the efficiency of H_2O_2 preparation (Fig. 12b–f). Teng *et al.* prepared Sb SAPCs using a bottom-up approach and used this photocatalyst to prepare H_2O_2.[79] The H_2O_2 yield of Sb SAPC is about 248 times higher than that of the original PCN, although testing shows that the surface area of Sb SAPC is only 1/7.78 of the original PCN, indicating that the enhanced activity per area of PCN after introducing single atom Sb is more than 1900 times higher than that of the original PCN. The generation of H_2O_2 through photocatalysis has great value for environmental development. The combination of single atoms and 2D materials for photocatalytic preparation can improve the selectivity and production efficiency of H_2O_2. However, there is still limited research in this area, and further in-depth research on its performance is needed.

To date, extensive research has been dedicated to the design and investigation of various SACs-2D catalysts aimed at enhancing photocatalytic efficacy. Table 1 lists the critical

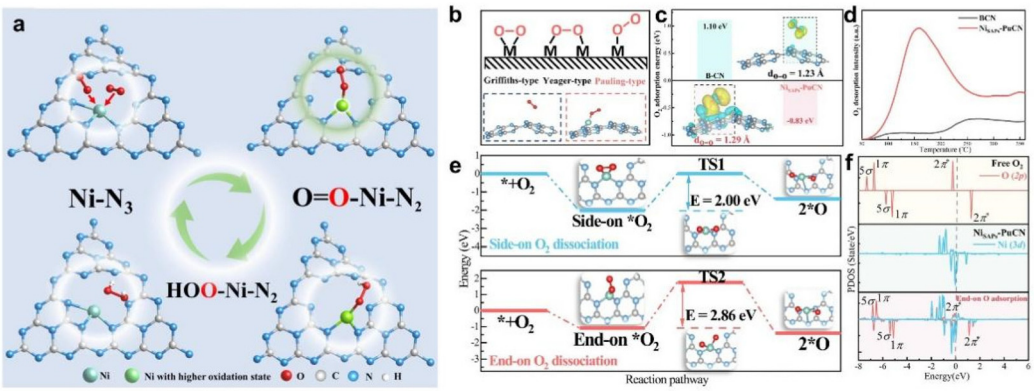

Fig. 12 (a) Mechanism diagram of bond changes in NiSAPs-PuCN during photocatalytic process, (b) Diagrammatic depiction of the O_2 adsorption framework, (c) O_2 adsorption energy on BCN and NiSAPS-PuCN catalysts, (d) O_2 desorption temperature profiles for BCN and NiSAPS-PuCN catalysts. (e) Reaction pathway for side-on and end-on O_2 dissociation on NiSAPs-PuCN catalysts. (f) The PDOS diagrams for O_2 in its unbounded state, NiSAPs-PuCN and NiSAPs-PuCN after end-on O_2 adsorption. Reproduced with permission.[20] Copyright 2023, Springer Nature.

Table 1 Recent research on SACs-2D photocatalysts

Photocatalysts	Reaction conditions	Application	Photocatalytic efficiencies	Ref.
Pt-TiO_2	20 mg photocatalyst, 20 mL methanol, 80 mL H_2O, 300 W Xe lamp	H_2 generation	52 720 μmol g^{-1} h^{-1}	3
Cu-TiO_2	20 mg photocatalyst, 120 mL of H_2O/methanol, Xe lamp light with intensity of 500 W m^{-2}	H_2 generation	101.7 mmol g^{-1} h^{-1}	84
Pt-C_3N_4	30 mg photocatalyst, 100 mL water, Xe lamp light with intensity of 100 mW cm^{-2}	H_2 generation	140 μmol g^{-1} h^{-1}	82
Ce-C_3N_4	30 mg photocatalyst, 90 mL water, 10 mL TEOA, Xe lamp light with intensity of 100 mW cm^{-2}	H_2 generation	33.5 mmol g^{-1} h^{-1}	26
Pd-C_3N_4	10 mg photocatalyst, 45 mL water, 5 mL TEOA, 300 W Xe lamp	H_2 generation	24.1 mmol g^{-1} h^{-1}	98
Pd-Co_3O_4	3 mg photocatalyst, CO_2, Xe lamp light with intensity of 100 mW cm^{-2}	CO_2 reduction	13.8 μmol g^{-1} h^{-1} (CH_3COOH)	88
Co-$Bi_{24}O_{31}Br_{10}$	30 mg photocatalyst, 50 ml water,0.08 MPa CO_2, 300 W Xe lamp	CO_2 reduction	43.4 μmol g^{-1} h^{-1} (CO)	40
Pd-CeO_2	5 mg photocatalyst, 10 ml water, CO_2, Xe lamp light with intensity of 100 mW cm^{-2}	CO_2 reduction	41.6 μmol g^{-1} h^{-1} (CH_4)	68
Au-$ZnIn_2S_4$	5 mg photocatalyst, 10 mg $Ru(bpy)_3Cl_2{\cdot}6H_2O$, 3 mL CH_3CN, 1 mL H_2O, 1 mL TEOA, CO_2, 300 W Xe lamp	CO_2 reduction	275 μmol g^{-1} h^{-1} (CH_4)	39
Pd_7Cu_1-TiO_2	5 mg photocatalyst, CO_2, 300 W Xe lamp	CO_2 reduction	19.6 μmol g^{-1} h^{-1} (CH_4)	69
Ag/mpg-C_3N_4	0.1 g L^{-1} photocatalyst, 1 mM PMS, 300 W Xe lamp	Organic pollutant degradation	100% of BPA are degraded within 60 min	25
Ce-Bi_2WO_6	0.6 g L^{-1} photocatalyst, 35 mg L^{-1} TCH, 20 mL L^{-1} oxidizing agent, 500 W Xe lamp	Organic pollutant degradation	90.4% of TCH are degraded within 40 min	92
Ru-CuO	10 mg photocatalyst, 20 ml water, N_2, 300 W Xe lamp	N_2 reduction	306 μmol g^{-1} h^{-1} (NH_3)	97
Mo-C_3N_4	3 mg photocatalyst, 6 ml water, N_2, 300 W Xe lamp	N_2 reduction	830 μmol g^{-1} h^{-1} NH_3	22
Cu-$Bi_{24}O_{31}Br_{10}$	50 mg photocatalyst, 100 ml water, N_2, 300 W Xe lamp	N_2 reduction	291.1 μmol g^{-1} h^{-1} NH_3	37
Ni-C_3N_4	30 mg photocatalyst, 30 ml pure water, O_2, 300 W Xe lamp	H_2O_2 generation	640.1 μmol L^{-1} h^{-1}	20
Sb-C_3N_4	100 mg photocatalyst, 50 ml water, O_2, 300 W Xe lamp	H_2O_2 generation	6.2 mg L^{-1} h^{-1}	79

information which facilitates a systematic comparison of these typical materials. It describes essential attributes such as sample name, reaction conditions, applications, and pivotal photocatalytic efficiencies. The objective of these data is to provide researchers with a comprehensive and clear perspective.

5. Summary and outlook

In this review, we summarize the latest advancements in combining single atoms with 2D materials for photocatalysis. The advantages of 2D materials, single atoms, and SACs-2D materials are introduced, and the approaches for the synthesis of SACs-2D materials, including wet chemistry, atomic layer deposition, and thermal decomposition, are described. The specific roles of SACs-2D materials in the photocatalytic process are summarized, including expanding the light absorption range, enhancing the carrier isolation efficiency, and accelerating the redox kinetics. Finally, the photocatalytic applications of SACs-2D materials have been surveyed, such as H_2 generation, CO_2 reduction, organic pollutant degradation, N_2 reduction, and H_2O_2 generation.

Despite some progress in the study of combining single atoms with 2D materials for photocatalysis, there are still many challenges to be overcome and solved. Firstly, the most common problem is the stability of single-atom sites. Under photocatalytic conditions, single atoms aggregate into less active clusters or nanoscale particles during synthesis and application. Specific annealing conditions, low-light conditions, and dry argon environment may reduce the aggregation probability, but this makes the photocatalytic conditions harsh, so new methods need to be developed to improve single-atom site stability. Secondly, how to achieve controllability of SACs-2D material synthesis. Although many synthesis methods are capable of attaining high loading capacity of single atoms, it is not easy to effectively modulate the count of active sites, and the active sites may not follow a uniform distribution, so the development of controllable, convenient, and economical SACs-2D material synthesis methods is an urgent requirement in this field. Thirdly, SACs-2D materials may lack selectivity for some specific products. Different kinds of single atoms can be considered to be introduced into 2D materials, or other newly developed 2D materials can be used as potential carriers for anchoring single atoms, or new development methods can be investigated, such as dual single atoms doping, the addition of two different single atoms to the same 2D material carrier, and the synergistic effect between them can be utilized to improve the product selectivity and photocatalytic performance of the photocatalysts. Fourthly, the role played by the SACs-2D structure in photocatalysis needs to be further explored. So far, the roles of SACs-2D materials in photocatalysis have been mainly focused on expanding the light absorption range, enhancing the carrier isolation efficiency, and accelerating the redox kinetics, but there are still many potential roles that have not been fully explored, for example, the lack of in-depth investigation on the electronic structure properties of the single atoms with the two-dimensional materials to reveal more advantages. Finally, the evolution of inexpensive, mass-production synthesis procedures.

Currently studied methods are often complex and consume significant time, so we need to seek a straightforward and efficient approach to prepare SACs-2D materials on a large scale. Rational design of industrial-scale single-atom photocatalyst reaction equipment is needed to adjust to diverse catalytic reaction conditions. Considering the practical elements such as light generator, temperature, catalyst regeneration, reactor pressure, and catalytic reaction efficiency, the transition from the laboratory scale to the pilot or even industrial scale remains significantly challenging. Despite the duration of this process, it is the essential step towards achieving its true implementation in industry.

Data availability

No primary research results, software or code have been included and no new data were generated or analysed as part of this review.

Conflicts of interest

There are no conflicts to declare.

Acknowledgements

This work was supported by the National Natural Science Foundation of China (No. 22378206, 22205108) and the Jiangsu Specially Appointed Professorship, Fundamental Research Funds for the Central Universities (No. 30922010302).

References

1 C. Gao, J. X. Low, R. Long, T. T. Kong, J. F. Zhu and Y. J. Xiong, *Chem. Rev.*, 2020, **120**, 12175.
2 H. F. Wang, J. H. Zhang, X. Jin, X. Q. Wang, F. Zhang, J. R. Xue, Y. P. Li, J. M. Li and G. Q. Zhang, *J. Mater. Chem. A*, 2021, **9**, 7143.
3 Y. J. Chen, S. F. Ji, W. M. Sun, Y. P. Lei, Q. C. Wang, A. Li, W. X. Chen, G. Zhou, Z. D. Zhang, Y. Wang, L. R. Zheng, Q. H. Zhang, L. Gu, X. D. Han, D. S. Wang and Y. D. Li, *Angew. Chem., Int. Ed.*, 2020, **59**, 1295.
4 J. Di, C. Chen, Y. Wu, H. Chen, R. Long, J. Xiong, S. Li, L. Song, W. Jiang and Z. Liu, *Adv. Mater.*, 2024, **36**, 2401914.
5 B. Wang, H. R. Cai and S. H. Shen, *Small Methods*, 2019, **3**, 1800447.
6 H. Q. Wang, Z. H. Chen, Y. R. Shang, C. D. Lv, X. H. Zhang, F. Li, Q. Z. Huang, X. D. Liu, W. M. Liu, L. Zhao, L. Q. Ye, H. Q. Xie and X. L. Jin, *ACS Catal.*, 2024, **14**, 5779.
7 B. C. Zhao, J. Y. Fu, C. L. Zhou, L. M. Yu and M. Qiu, *Small*, 2023, **19**, 2301917.
8 C. Liu, P. Zhao, K. R. Lu, S. Han, C. Zhang, X. F. Xia, W. Lei, Q. B. Guo and Q. L. Hao, *Adv. Funct. Mater.*, 2024, 2401392.
9 H. J. Peng, S. H. Huang, V. Montes-García, D. Pakulski, H. P. Guo, F. Richard, X. D. Zhuang, P. Samorì and A. Ciesielski, *Angew. Chem., Int. Ed.*, 2023, **62**, 202216136.
10 C. Fox, Y. L. Mao, X. Zhang, Y. Wang and J. Xiao, *Chem. Rev.*, 2023, **124**, 1862.
11 L. Tang and J. Zou, *Nano-Micro Lett.*, 2023, **15**, 230.
12 S. S. T. Nibhanupudi, A. Roy, D. Veksler, M. Coupin, K. C. Matthews, M. Disiena, J. V. Singh, I. R. Gearba-Dolocan, J. Warner, J. P. Kulkarni, G. Bersuker and S. K. Banerjee, *Nat. Commun.*, 2024, **15**, 2334.
13 Y. J. Fan, D. W. Kang, S. Labalme and W. B. Lin, *J. Am. Chem. Soc.*, 2023, **145**, 25074.
14 H. Xia, X. Sang, Z. Shu, Z. Shi, Z. Li, S. Guo, X. An, C. Gao, F. Liu, H. Duan, Z. Liu and Y. He, *Nat. Commun.*, 2023, **14**, 6838.
15 Y. C. Kong, X. S. Li, A. R. P. Santiago and T. W. He, *J. Am. Chem. Soc.*, 2024, **146**, 5987.
16 Y. H. Liu, Y. Wang, J. Shang, J. Peng and T. Zhu, *Appl. Catal., B*, 2024, **350**, 123937.
17 R. J. Yang, Y. Y. Fan, Y. F. Zhang, L. Mei, R. S. Zhu, J. Q. Qin, J. G. Hu, Z. X. Chen, Y. H. Ng, D. Voiry, S. Li, Q. Y. Lu, Q. Wang, J. C. Yu and Z. Y. Zeng, *Angew. Chem., Int. Ed.*, 2023, **62**, 202218016.
18 M. Ikram, A. Raza, S. O. A. Ahmad, A. Ashfaq, M. U. Akbar, M. Imran, S. Dilpazir, M. Khan, Q. Khan and M. Maqbool, *Adv. Mater. Interfaces*, 2023, **10**, 2202172.
19 T. Li, H. W. Huang, S. B. Wang, Y. Mi and Y. H. Zhang, *Nano Res.*, 2023, **16**, 8542.
20 X. Zhang, H. Su, P. X. Cui, Y. Y. Cao, Z. Y. Teng, Q. T. Zhang, Y. Wang, Y. B. Feng, R. Feng, J. X. Hou, X. Y. Zhou, P. J. Ma, H. W. Hu, K. W. Wang, C. Wang, L. Y. Gan, Y. X. Zhao, Q. H. Liu, T. R. Zhang and K. Zheng, *Nat. Commun.*, 2023, **14**, 7115.
21 C. Y. Ling, X. H. Niu, Q. Li, A. J. Du and J. L. Wang, *J. Am. Chem. Soc.*, 2018, **140**, 14161.
22 X. W. Guo, S. M. Chen, H. J. Wang, Z. M. Zhang, H. Lin, L. Song and T. B. Lu, *J. Mater. Chem. A*, 2019, **7**, 19831.
23 H. Su, W. Che, F. M. Tang, W. R. Cheng, X. Zhao, H. Zhang and Q. H. Liu, *J. Phys. Chem. C*, 2018, **122**, 21108.
24 J. W. Fu, S. D. Wang, Z. H. Wang, K. Liu, H. J. W. Li, H. Liu, J. H. Hu, X. W. Xu, H. M. Li and M. Liu, *Front. Phys.*, 2020, **15**, 1.
25 Y. B. Wang, X. Zhao, D. Cao, Y. Wang and Y. F. Zhu, *Appl. Catal., B*, 2017, **211**, 79.
26 D. Sun, Y. J. Chen, X. Y. Yu, Y. J. Yin and G. H. Tian, *Chem. Eng. J.*, 2023, **462**, 142084.
27 H. H. Zhai, P. F. Tan, M. Jiang, M. Y. Zhang, R. F. Ren, R. Sa and J. Pan, *ACS Catal.*, 2023, **13**, 8063.
28 Y. R. Shang, M. Zheng, H. J. Liu, X. L. Jin, C. S. Yan, L. Song, Z. M. Qi, F. Y. Jing, P. Song, X. Zhou, G. Chen and C. D. Lv, *ACS Catal.*, 2023, **13**, 14530.
29 Y. R. Shang, Y. J. Hou, X. Cao, H. J. Liu, X. L. Jin, J. W. Liu, C. S. Yan, Y. M. Qian, L. Song, Z. M. Qi, P. Song, Y. S. Zhou,

D. B. Liu, Z. Liu, F. Y. Jing, Q. Y. Yan, G. Chen and C. D. Lv, *Chem. Eng. J.*, 2024, **486**, 150306.
30 Y. R. Shang, C. L. Wang, C. S. Yan, F. Y. Jing, M. Roostaeinia, Y. Wang, G. Chen and C. D. Lv, *J. Colloid Interface Sci.*, 2023, **634**, 195.
31 Q. Zhao, W. F. Yao, C. P. Huang, Q. Wu and Q. J. Xu, *ACS Appl. Mater. Interfaces*, 2017, **9**, 42734.
32 S. Liu, Y. Wang, S. Wang, M. You, S. Hong, T.-S. Wu, Y.-L. Soo, Z. Zhao, G. Jiang, J. Qiu, B. Wang and Z. Sun, *ACS Sustainable Chem. Eng.*, 2019, **7**, 6813.
33 S. M. Wu, I. Hwang, B. Osuagwu, J. Will, Z. N. Wu, B. B. Sarma, F. F. Pu, L. Y. Wang, Z. Badura, G. Zoppellaro, E. Spiecker and P. Schmuki, *ACS Catal.*, 2023, **13**, 33.
34 S. Hejazi, S. Mohajernia, B. Osuagwu, G. Zoppellaro, P. Andryskova, O. Tomanec, S. Kment, R. Zboril and P. Schmuki, *Adv. Mater.*, 2020, **32**, 1908505.
35 S. Ida, N. Kim, E. Ertekin, S. Takenaka and T. Ishihara, *J. Am. Chem. Soc.*, 2015, **137**, 239.
36 P. G. Liu, Z. X. Huang, S. K. Yang, J. Y. Du, Y. D. Zhang, R. Cao, C. Chen, L. Li, T. Chen, G. M. Wang, D. W. Rao, X. S. Zheng and X. Hong, *ACS Catal.*, 2022, **12**, 8139.
37 J. Di, C. Chen, Y. Wu, Y. X. Zhao, C. Zhu, Y. Zhang, C. D. Wang, H. L. Chen, J. Xiong, M. Z. Xu, J. X. Xia, J. D. Zhou, Y. X. Weng, L. Song, S. Z. Li, W. Jiang and Z. Liu, *Adv. Mater.*, 2022, **34**, 2204959.
38 J. R. Ran, L. Chen, D. Y. Wang, A. Talebian-Kiakalaieh, Y. Jiao, M. A. Hamza, Y. Qu, L. Q. Jing, K. Davey and S. Z. Qiao, *Adv. Mater.*, 2023, **35**, 2210164.
39 S. H. Si, H. W. Shou, Y. Y. Mao, X. L. Bao, G. Y. Zhai, K. P. Song, Z. Y. Wang, P. Wang, Y. Y. Liu, Z. K. Zheng, Y. Dai, L. Song, B. B. Huang and H. F. Cheng, *Angew. Chem., Int. Ed.*, 2022, **61**, 202209446.
40 M. Zhang, Y. Wu, X. Zhu, P. Song, H. Chen, J. Xiong and J. Di, *ACS Mater. Lett.*, 2024, **6**, 2626.
41 Y. Zhang, Z. H. Li, K. Chen, X. Yang, H. Zhang, X. J. Liu and K. Chu, *Adv. Energy Mater.*, 2024, DOI: **10.1002/aenm.202402309**.
42 W. Q. Zhang, X. H. Qin, T. R. Wei, Q. Liu, J. Luo and X. J. Liu, *J. Colloid Interface Sci.*, 2023, **638**, 650.
43 X. C. Jiao, K. Zheng, L. Liang, X. D. Li, Y. F. Sun and Y. Xie, *Chem. Soc. Rev.*, 2020, **49**, 6592.
44 X. J. Shi, L. N. Y. Cao, M. J. Chen and Y. Huang, *Chin. Chem. Lett.*, 2022, **33**, 5023.
45 P. P. Huang, J. H. Huang, S. A. Pantovich, A. D. Carl, T. G. Fenton, C. A. Caputo, R. L. Grimm, A. I. Frenkel and G. H. Li, *J. Am. Chem. Soc.*, 2018, **140**, 16042.
46 J. Xing, J. F. Chen, Y. H. Li, W. T. Yuan, Y. Zhou, L. R. Zheng, H. F. Wang, P. Hu, Y. Wang, H. J. Zhao, Y. Wang and H. G. Yang, *Chemistry*, 2014, **20**, 2138.
47 W. A. Qureshi, S. Haider, A. Naveed, A. Ali, Q. Q. Liu and J. Yang, *Int. J. Hydrogen Energy*, 2023, **48**, 19459.
48 Y. J. Cao, S. Chen, Q. Q. Luo, H. Yan, Y. Lin, W. Liu, L. L. Cao, J. L. Lu, J. L. Yang, T. Yao and S. Q. Wei, *Angew. Chem., Int. Ed.*, 2017, **56**, 12191.
49 R. Shi, C. C. Tian, X. Zhu, C. Y. Peng, B. B. Mei, L. He, X. L. Du, Z. Jiang, Y. Chen and S. Dai, *Chem. Sci.*, 2019, **10**, 2585.
50 S. Hu, P. Z. Qiao, X. M. Liang, G. M. Ba, X. L. Zu, H. L. Hu, J. H. Ye and D. F. Wang, *Appl. Catal., B*, 2024, **346**, 123737.
51 C. M. Zhao, X. Y. Dai, T. Yao, W. X. Chen, X. Q. Wang, J. Wang, J. Yang, S. Q. Wei, Y. E. Wu and Y. D. Li, *J. Am. Chem. Soc.*, 2017, **139**, 8078.
52 L. Ma, R. F. Guan, W. X. Kang, Z. Sun, H. M. Li, Q. R. Li, Q. Q. Shen, C. Q. Chen, X. G. Liu, H. S. Jia and J. B. Xue, *J. Colloid Interface Sci.*, 2024, **660**, 381.
53 F. Dong, X. Liang, Z. D. Zhang, H. B. Yin, D. S. Wang, J. H. Li and Y. D. Li, *Adv. Mater.*, 2024, **36**, 2401055.
54 X. Chen and C. Burda, *J. Am. Chem. Soc.*, 2008, **130**, 5018.
55 T. Tong, B. He, B. Zhu, B. Cheng and L. Zhang, *Appl. Surf. Sci.*, 2018, **459**, 385.
56 J. Di, C. Chen, S. Z. Yang, S. M. Chen, M. L. Duan, J. Xiong, C. Zhu, R. Long, W. Hao, Z. Chi, H. L. Chen, Y. X. Weng, J. X. Xia, L. Song, S. Z. Li, H. M. Li and Z. Liu, *Nat. Commun.*, 2019, **10**, 2840.
57 J. M. Luo, H. A. Han, X. L. Wang, X. Z. Qiu, B. Liu, Y. L. Lai, X. Y. Chen, R. M. Zhong, L. Wang and C. Y. Wang, *Appl. Catal., B*, 2023, **328**, 122495.
58 S. H. Si, H. W. Shou, Y. Y. Mao, X. L. Bao, G. Y. Zhai, K. P. Song, Z. Y. Wang, P. Wang, Y. Y. Liu, Z. K. Zheng, Y. Dai, L. Song, B. B. Huang and H. F. Cheng, *Angew. Chem., Int. Ed.*, 2022, **61**, e202209446.
59 C. Chen, C. Y. Ye, X. L. Zhao, Y. Z. Zhang, R. L. Li, Q. Zhang, H. Zhang and Y. Wu, *Nat. Commun.*, 2024, **15**, 7825.
60 S. A. Yue, Z. Y. Zhao, T. Zhang, P. F. Wang and S. H. Zhan, *Mater. Today Energy*, 2024, **40**, 101482.
61 Y. Liu, J. H. Sun, H. H. Huang, L. L. Bai, X. M. Zhao, B. H. Qu, L. Q. Xiong, F. Q. Bai, J. W. Tang and L. Q. Jing, *Nat. Commun.*, 2023, **14**, 1457.
62 Y. J. Yuan, N. Lu, L. Bao, R. Tang, F. G. Zhang, J. Guan, H. D. Wang, Q. Y. Liu, Q. Cheng, Z. T. Yu and Z. G. Zou, *ACS Nano*, 2022, **16**, 12174.
63 P. G. Liu, Z. X. Huang, S. K. Yang, J. Y. Du, Y. D. Zhang, R. Cao, C. Chen, L. Li, T. Chen, G. M. Wang, D. W. Rao, X. S. Zheng and X. Hong, *ACS Catal.*, 2022, **12**, 8139–8146.
64 J. C. Shen, C. H. Luo, S. S. Qiao, Y. Q. Chen, Y. H. Tang, J. Q. Xu, K. X. Fu, D. W. Yuan, H. F. Tang, H. Zhang and C. B. Liu, *ACS Catal.*, 2023, **13**, 6280.
65 P. Zhou, F. Lv, N. Li, Y. L. Zhang, Z. J. Mu, Y. H. Tang, J. P. Lai, Y. G. Chao, M. C. Luo, F. Lin, J. H. Zhou, D. Su and S. J. Guo, *Nano Energy*, 2019, **56**, 127.
66 Y. L. Wang, H. B. Yin, X. G. Zhao, Y. K. Qu, A. G. Zheng, H. Zhou, W. Fang and J. H. Li, *Appl. Catal., B*, 2024, **341**, 123266.
67 Y. J. Cao, D. H. Wang, Y. Lin, W. Liu, L. L. Cao, X. K. Liu, W. Zhang, X. L. Mou, S. Fang, X. Y. Shen and T. Yao, *ACS Appl. Energy Mater.*, 2018, **1**, 6082.
68 Z. Q. Wang, J. C. Zhu, X. L. Zu, Y. Wu, S. Shang, P. Q. Ling, P. Z. Qiao, C. Y. Liu, J. Hu, Y. Pan, J. F. Zhu, Y. F. Sun and Y. Xie, *Angew. Chem., Int. Ed.*, 2022, **61**, 202203249.
69 R. Long, Y. Li, Y. Liu, S. M. Chen, X. S. Zheng, C. Gao, C. H. He, N. S. Chen, Z. M. Qi, L. Song, J. Jiang, J. F. Zhu and Y. J. Xiong, *J. Am. Chem. Soc.*, 2017, **139**, 4486.

70 L. Q. Xiong, H. F. Qi, S. X. Zhang, L. L. Zhang, X. Y. Liu, A. Q. Wang and J. W. Tang, *Adv. Mater.*, 2023, **35**, 202209646.
71 X. C. Liu, M. Mateen, X. K. Cheng, D. Q. Wu, J. Zhang, W. C. Cheong and S. J. Liu, *Int. J. Hydrogen Energy*, 2022, **47**, 12592.
72 Q. Zuo, T. T. Liu, C. S. Chen, Y. Ji, X. Q. Gong, Y. Y. Mai and Y. F. Zhou, *Angew. Chem., Int. Ed.*, 2019, **58**, 10198.
73 S. C. Lv, M. X. Pei, Y. X. Liu, Z. C. Si, X. D. Wu, R. Ran, D. Weng and F. Y. Kang, *Nano Res.*, 2022, **15**, 5848.
74 G. W. Yin, C. X. Zhang, Y. D. Liu, Y. P. Sun and X. Qi, *Nanomaterials*, 2024, **14**, 1183.
75 W. Y. Pan, Z. H. Wei, Y. H. Su, Y. B. Lian, Z. Y. Zheng, H. H. Yuan, Y. Z. Qin, X. L. Xie, Q. Q. Bai, Z. Y. Jiao, W. Hua, J. Z. Chen, W. J. Yang, Z. Deng and Y. Peng, *Nano Res.*, 2024, **17**, 2410.
76 C. L. Tan, M. Y. Qi, Z. R. Tang and Y. J. Xu, *ACS Catal.*, 2023, **13**, 8317.
77 F. X. Wang, C. C. Wang, X. D. Du, Y. Li, F. Wang and P. Wang, *Chem. Eng. J.*, 2022, **429**, 132495.
78 A. N. Singh, R. Anand, M. Zafari, M. Ha and K. S. Kim, *Adv. Energy Mater.*, 2024, **14**, 2304106.
79 Z. Y. Teng, Q. T. Zhang, H. B. Yang, K. Kato, W. J. Yang, Y. R. Lu, S. X. Liu, C. Y. Wang, A. Yamakata, C. L. Su, B. Liu and T. Ohno, *Nat. Catal.*, 2021, **4**, 374.
80 Y. J. Chen, S. F. Ji, C. Chen, Q. Peng, D. S. Wang and Y. D. Li, *Joule*, 2018, **2**, 1242.
81 T. Hisatomi and K. Domen, *Nat. Catal.*, 2019, **2**, 387.
82 X. G. Li, W. T. Bi, L. Zhang, S. Tao, W. S. Chu, Q. Zhang, Y. Luo, C. Z. Wu and Y. Xie, *Adv. Mater.*, 2016, **28**, 2427.
83 J. Di and W. Jiang, *Mater. Today Catal.*, 2023, **1**, 100001.
84 Y. M. Zhang, J. H. Zhao, H. Wang, B. Xiao, W. Zhang, X. B. Zhao, T. P. Lv, M. Thangamuthu, J. Zhang, Y. Guo, J. N. Ma, L. N. Lin, J. W. Tang, R. Huang and Q. J. Liu, *Nat. Commun.*, 2022, **13**, 2062.
85 C. Liao, W. H. Jing, F. Wang and Y. Liu, *Mater. Today Catal.*, 2023, **3**, 100030.
86 C. B. Hiragond, N. S. Powar, J. Lee and S. I. In, *Small*, 2022, **18**, 2201428.
87 C. Gao, S. M. Chen, Y. Wang, J. W. Wang, X. S. Zheng, J. F. Zhu, L. Song, W. K. Zhang and Y. J. Xiong, *Adv. Mater.*, 2018, **30**, 1704624.
88 J. Y. Ding, P. J. Du, J. C. Zhu, Q. Hu, D. P. He, Y. Wu, W. X. Liu, S. Zhu, W. S. Yan, J. Hu, J. F. Zhu, Q. X. Chen, X. C. Jiao and Y. Xie, *Angew. Chem., Int. Ed.*, 2024, **63**, 202400828.
89 Y. Li, B. H. Li, D. N. Zhang, L. Cheng and Q. J. Xiang, *ACS Nano*, 2020, **14**, 10552.
90 M. Xie, J. C. Tang, L. S. Kong, W. H. Lu, V. Natarajan, F. Zhu and J. H. Zhan, *Chem. Eng. J.*, 2019, **360**, 1213.
91 Y. L. Pang, A. Z. Abdullah and S. Bhatia, *Desalination*, 2011, **277**, 1.
92 H. Zhang, W. Luo, H. Sun, H. Yang, T. Yang, D. Liu, X. Zhu, L. Zhao, M. Shu and F. Yang, *ACS Appl. Nano Mater.*, 2024, **7**, 11506–11517.
93 C. Zhu, L. Lu, Q. L. Fang, S. Song, B. L. Chen and Y. Shen, *Adv. Funct. Mater.*, 2023, **33**, 2210905.
94 K. Chen, D. Y. Ma, Y. Zhang, F. Z. Wang, X. Yang, X. M. Wang, H. Zhang, X. J. Liu, R. Bao and K. Chu, *Adv. Mater.*, 2024, **36**, 2402160.
95 C. J. M. van der Ham, M. T. M. Koper and D. G. H. Hetterscheid, *Chem. Soc. Rev.*, 2014, **43**, 5183.
96 H. Ali, M. Masar, A. C. Guler, M. Urbanek, M. Machovsky and I. Kuritka, *Nanoscale Adv.*, 2021, **3**, 6358.
97 Y. D. Zhang, Q. Y. Wang, S. K. Yang, H. W. Wang, D. W. Rao, T. Chen, G. M. Wang, J. L. Lu, J. F. Zhu, S. Q. Wei, X. S. Zheng and J. Zeng, *Adv. Funct. Mater.*, 2022, **32**, 2112452.
98 M. Ren, J. Q. Meng, Y. X. Yang, X. Y. Zhang, G. Yang, L. Qin and Y. H. Guo, *Appl. Catal., B*, 2024, **345**, 123680.